HHS Public Access

Author manuscript

Sci Transl Med. Author manuscript; available in PMC 2024 August 01.

Published in final edited form as:

Sci Transl Med. 2023 September 27; 15(715): eadg5567. doi:10.1126/scitranslmed.adg5567.

A MERS-CoV Antibody Neutralizes a Pre-emerging Group 2c Bat Coronavirus

Longping V. Tse[*,1], **Yixuan J. Hou**[*,2], **Elizabeth McFadden**[3], **Rhianna E Lee**[4], **Trevor D. Scobey**[2], **Sarah R. Leist**[2], **David R. Martinez**[2], **Rita M. Meganck**[1], **Alexandra Schäfer**[2], **Boyd L. Yount**[2], **Teresa Mascenik**[4], **John M. Powers**[2], **Scott H Randell**[4], **Yi Zhang**[5], **Lingshu Wang**[5], **John Mascola**[5], **Jason S. McLellan**[3], **Ralph S. Baric**[2,†]

[1]Department of Molecular Microbiology and Immunology, Saint Louis University, St. Louis, MO 63014

[2]Department of Epidemiology, University of North Carolina at Chapel Hill, Chapel Hill, NC 27599

[3]Department of Molecular Biosciences, The University of Texas at Austin, Austin, TX 78712

[4]Marsico Lung Institute, University of North Carolina at Chapel Hill, Chapel Hill, NC 27599

[5]National Institute of Allergy and Infectious Disease, National Institute of Health, Bethesda, MD 20892

Abstract

The repeated emergence of zoonotic human betacoronaviruses (β-CoVs) dictates the need for broad therapeutics and conserved epitope targets for countermeasure design. Middle East respiratory syndrome (MERS)-related coronaviruses (CoVs) remain a pressing concern for global health preparedness. Using metagenomic sequence data and CoV reverse genetics, we recovered a full-length wildtype MERS-like BtCoV/*li*/GD/2014–422 (BtCoV-422) recombinant virus, as well as two reporter viruses, and evaluated their human emergence potential and susceptibility to currently available countermeasures. Like MERS-CoV, BtCoV-422 efficiently utilized human and other mammalian dipeptidyl peptidase-4 (DPP4) proteins as entry receptors and an alternative DPP4-independent infection route in the presence of exogenous proteases. BtCoV-422 also replicated efficiently in primary human airway, lung endothelial, and fibroblast cells, although less efficiently than MERS-CoV. However, BtCoV-422 shows minor signs of infection in 288/330

[†]Corresponding author: rbaric@email.unc.edu.

Author Contributions: L.V.T., Y.J.H., and R.S.B. designed the study. L.V.T., Y.J.H., E.M., R.E.L., T.D.S., S.R.L., D.R.M., R.M.M., A.S., B.L.Y., T.M., J.M.P. performed experiments. E.M. and J.S.M. perform cryo-EM experiments. R.E.L., and T.M. performed staining and confocal microscopy of primary airway cultures. S.R.L. performed animal experiments. R.E.L. and S.H.R. provided primary airway cultures. Y.Z., L.W., J.M., and J.S.M., provided reagents. R.S.B. provided oversight of the project and funding. L.V.T. wrote the manuscript. L.V.T., Y.J.H., and R.B.S. reviewed and revised the final version. All authors approved the final version of the manuscript.

[*]These authors contributed equally

Supplemental Materials

Fig. S1 to S7

Table S1

MDAR Reproducibility Checklist

Data file S1

Competing Interests: R.S.B. is a member of the Scientific Advisory Board of Invivyd and VaxArt and has consulted on virus-related countermeasures with Gilead, Moderna, Takeda, BioNet and Janssen Bio that are unrelated to this project.

human DPP4 transgenic mice. Several broad CoV antivirals, including nucleoside analogues and 3C-like/M^{pro} protease inhibitors, demonstrated potent inhibition against BtCoV-422 in vitro. Serum from mice that received a MERS-CoV mRNA vaccine showed reduced neutralizing activity against BtCoV-422. Although most MERS-CoV neutralizing monoclonal antibodies (mAbs) had limited activity, one anti-MERS receptor binding domain mAb, JC57–11, neutralized BtCoV-422 potently. A cryo-electron microscopy structure of JC57–11 in complex with BtCoV-422 spike protein revealed the mechanism of cross neutralization involving occlusion of the DPP4 binding site, highlighting its potential as a broadly neutralizing mAb for group 2c CoVs that use DPP4 as a receptor. These studies provide critical insights into MERS-like CoVs and provide candidates for countermeasure development.

One-sentence summary:

JC57–11 shows neutralization efficacy against an emerging group 2c BtCoV-422 strain that replicates in primary human airway cells.

Introduction

Coronaviruses (CoV) infect a wide range of animals and rapidly adapt and spread in different species, with the potential to establish endemic infections within human and animal populations (1). In 2002, severe acute respiratory syndrome coronavirus-1 (SARS-CoV) emerged from high-risk sarbecoviruses circulating in bat and animal reservoirs, heralding the human threat potential of emerging coronaviruses (1–4). In 2019, SARS-CoV-2 emerged from zoonotic reservoirs to cause coronavirus disease 2019 (COVID-19), then rapidly evolved into multiple variants of concern (VOCs) that fueled the ongoing global pandemic (1, 2). In 2012, Middle East respiratory syndrome coronavirus (MERS-CoV) emerged, with an estimated 35% mortality rate in infected patients, leading to at least 945 deaths (3, 5). Zoonotic transmission events were largely associated with close contact between human and intermediate camel hosts; human-to-human transmission was tied to close household contact and health care settings (6). As of 2022, MERS-CoV is still causing sporadic cases reported in the Middle East and elsewhere (7).

Bats are a reservoir for a vast number of viruses, and fuel zoonotic transmission of CoVs to other mammals, including humans. For instance, swine acute diarrhea syndrome coronavirus (SADS-CoV), which caused multiple outbreaks in China, originated from a strain closely related to bat CoV-HKU2 (8). Although definitive evidence is lacking, molecular clock analysis suggests that Porcine Epidemic Diarrhea Virus (PEDV) (9), human coronavirus (hCoV)-NL63 (10), and hCoV-229E (11) all originated from bat CoVs, whereas the hCoV OC43 likely originated from cattle (12). As such, understanding the properties and molecular tropism of zoonotic CoVs is important for risk management of potential zoonotic transmission. Originating from reservoirs circulating in bats, MERS-CoV is representative of several group 2c merbecoviruses, including those found in *Tylonycteris* bats (BtCoV-HKU4), *Pipistrellus* bats (BtCoV-HKU5), and *Ia io* bats (BtCoV/*Ii*/GD/2014-422) (BtCoV-422) (13, 14). Recently, a MERS-like CoV, MjHKU4r-CoV-1, was isolated from pangolins, indicating the widespread host range of MERS-like CoVs (15). MERS-CoV uses camel and human dipeptidyl peptidase protein 4 (DPP4) as a receptor,

and host furin for spike protein activation, allowing efficient replication in humans (16–18). However, adaptation is a multi-faceted process in which a variety of pathways may lead to inter-species tropism switches. For instance, BtCoV-HKU4 can bind the human (h) DPP4 receptor and infect in the absence of external proteases (19); other MERS-like CoVs such as BtCoV-Uganda and BtCoV-HKU5 cross the species barrier using protease cleavage, as evident by the requirement of exogenous trypsin addition but not hDPP4 binding for in vitro replication (20). NeoCoV, a close relative of MERS-CoV, was reported to use angiotensin converting enzyme 2 (ACE2) as its cellular receptor (21). The plethora of available sequence information of MERS-like CoVs in wildlife is a great resource for understanding CoV adaptation pathways. Because the origin of MERS-CoV has not been identified, characterizing MERS-like CoVs serve as a gateway to identify the parental virus of MERS-CoV and other potential human emergent strains, as well as providing tools for testing broad spectrum antivirals and vaccines for pandemic preparedness.

In this report, we synthetically resurrected a MERS-like bat CoV, BtCoV-422 (14), that has 65% sequence identity with the RBD of MERS-CoV. We analyzed BtCoV-422 adaptation pathways by investigating its ability to use DPP4 entry receptors from multiple species, including humans, and its reliance on external proteases. We assessed replication efficiency of BtCoV-422 in multiple primary human cells including airway epithelia, lung fibroblasts, and lung endothelial cells. We then tested current countermeasures, including drugs, monoclonal antibodies (mAbs), and vaccine-elicited murine serum, as well as structurally characterized a group 2c CoV broadly cross-reactive epitope. These data inform future CoV global health preparedness strategies.

Results

Development of BtCoV-422 wildtype and reporter infectious clones

BtCoV-422 is a MERS-related CoV isolated from the great evening bat (*Ia io*), which, although rare, is distributed throughout southeast Asia and poses concern for zoonotic transmission (14). BtCoV-422 is a group 2c CoV and, along with BtCoV-HKU4 and BtCoV-HKU5, branches apart from MERS-CoV (Fig. 1A). The spike proteins of BtCoV-422 and MERS-CoV have 65% sequence identity overall, and 62% sequence identity in their receptor binding domains (RBDs) (Fig. 1B). Like other merbecoviruses, BtCoV-422 spike protein lacks the S1/S2 and S2′ furin cleavage sites seen in MERS-CoV and BtCoV-HKU5 (Fig. 1C). To better understand the biology and assess the pandemic potential of BtCoV-422, we used published sequences to synthetically derive a full-length, wildtype infectious clone using reverse genetics (22). We also recovered two replication competent reporter viruses by replacing ORF5 with either nano-luciferase (nLuc) or green fluorescent protein (GFP) (Fig. 1D). We successfully established all three viruses without any obvious replication defect in vitro as determined by virus yield at 120 hours post infection (hpi) and plaque morphology at 48 hpi in Vero cells (Fig. 1E and 1F).

BtCoV-422 infects distal, but not proximal, human airway cells.

MERS-CoV replicates efficiently in multiple primary cell types from the lung, including airway epithelial cells(23). Nasal epithelium is the first barrier for respiratory viruses

to overcome and establish infection, which serves as a good indicator of the potential for zoonotic transmission. We utilized primary human nasal epithelial cells (NE) from four different donors; 3 out of 4 donor cultures supported MERS-CoV replication [10^5 to 10^6 plaque-forming units (PFU)/mL] but have limited support to BtCoV-422 growth based on growth kinetics as no detectable infectious virus (Fig. 2A and 2B). Reporter protein expression showed that rare GFP (BtCoV-422) signal was observed in infected NEs, suggesting limited permissiveness in NE cells (Fig. 2A and 2B). Unlike nasal epithelia, human large airway epithelia (LAE) supported efficient replication of BtCoV-422, although the overall growth kinetics of BtCoV-422 were slower than MERS-CoV. BtCoV-422 reached a 2 to 3-log lower peak titer (10^5 PFU/mL) and took longer to reach peak titer (greater than 96 hours post-infection) than MERS-CoV (Fig. 2C). To evaluate virus tropism in LAE, we observed expression of nuclear protein (N) by immunofluorescence in both MERS-CoV and BtCoV-422 infected LAE cultures after 72 hpi (fig. S1 and S2). Both BtCoV-422 and MERS-CoV infected ciliated (white arrows) and non-ciliated (cyan arrows) airway epithelial cells (fig. S1 and S2). MERS-CoV shows a preference for non-ciliated cells on 2 out of 3 stained sections, as previously described in the literature (23). As expected, MERS-CoV infection was associated with the expression of its receptor, hDPP4 (fig. S2). In contrast, BtCoV-422 infected LAEs showed a weaker correlation with hDPP4 receptor expression (fig. S1). Earlier studies demonstrated that MERS-CoV replicates to high titers in lung fibroblasts and microvascular endothelial cells (MVEs) (23, 24). To further investigate the human airway tropism of BtCoV-422, we infected primary human lung MVEs and fibroblasts from two matched donors with BtCoV-422-GFP. BtCoV-422 infected MVEs from both donors, growing to intermediate titers of about 10^4 PFU/mL. GFP expression supported the finding that about 10% of MVEs had been productively infected (Fig. 2D). In contrast, only one of the fibroblast donor samples supported replication of BtCoV-422, with low virus titers peaking at about 10^3 PFU/mL (Fig. 2E). GFP expression revealed that approximately 40% of fibroblasts were infected with BtCoV-422, suggesting the potential for strain and tissue specific regulation of distinct merbecoviruses (24).

BtCoV-422 and MERS-CoV use a similar species profile of DPP4 as a receptor.

Emerging merbecoviruses appear to have a broad host range reflective of their capacity to engage multiple species' DPP4 receptor orthologs (17). Given the similarity of the spike proteins between BtCoV-422 and MERS-CoV, we hypothesized that BtCoV-422 would recognize multiple species of DPP4 ligands as entry receptors. We tested DPP4s from seven ecologically important species for MERS-related viruses on Vero cells. First, CRISPR/Cas9 was used to remove endogenous DPP4 expression from Vero cells. These clonally selected and sequence-verified Vero-DPP4 knockout (KO) cells were nonpermissive for BtCoV-422 and MERS-CoV infection, indicating that primate DPP4 (moDPP4) is a functional entry receptor for both strains (Fig. 3A and 3B). We then established stable cell lines that overexpressed DPP4 from other species on the Vero-DPP4 KO base (fig. S3). Among all the DPP4s tested, human, camel, monkey, and bat supported both BtCoV-422 and MERS-CoV infection. Direct comparison of receptor ortholog usage was complicated by variability in DPP4 expression across the panel, but still allows for receptor-specific comparison between MERS-CoV and BtCoV-422 (Fig. 3A and 3B). Of note, BtCoV-422 was more efficient at recognizing bat DPP4 than MERS-CoV, possibly reflecting co-evolution with its natural host

(Fig. 3A and 3B). In our system, ferret, guinea pig, hamster, and mouse DPP4 receptors did not rescue infection of either BtCoV-422 or MERS-CoV (Fig 3A and 3B), consistent with earlier studies (25, 26). Findings with nLuc reporter viruses supported the restricted host range for BtCoV-422 and MERS-CoV (Fig. 3C and 3D).

External proteases enhance BtCoV-422 replication in vitro.

The absence of furin cleavage sites in both S1/S2 and S2′ of BtCoV-422 suggests other host proteases may restrict entry and host range potential. Because most other group 2c CoVs require exogenous trypsin for efficient replication in vitro (20), we infected Caco-2, Calu-3, and Vero cells with BtCoV-422-nLuc in the presence of different exogenous proteases and measured infectivity by nLuc expression at 24 hpi. Addition of trypsin increased nLuc expression 5- to 10-fold in BtCoV-422 infected cell lines compared to the no protease control (Fig. 4A to C). Exogenous thermolysin increased expression in Caco-2 cells (Fig. 4A to C). No difference in BtCoV-422 infectivity was observed in the presence of elastase (Fig. 4A to C). To understand the replication kinetics, we examined BtCoV-422 growth on Vero cells in the presence of exogenous trypsin. The addition of trypsin did not enhance the peak yield (10^5 PFU/mL) of BtCoV-422, but reduced the time required to achieve peak titers from 96–120 hpi to 48 hpi (Fig. 4D). Trypsin addition also led to extensive syncytia formation at 48 hpi, coinciding with peak virus titers and followed by rapid decline (Fig. 4E and 4F).

BtCoV-422 uses a DPP4-independent entry pathway in the presence of trypsin.

Exogenous proteases may enhance replication in a receptor-dependent or independent manner. To address this question, we infected Vero-DPP4 KO cells with BtCoV-422 and MERS-CoV in the presence or absence of trypsin. As previously described, trypsin enhanced BtCoV-422 replication in wildtype Vero cells and initiated the formation of large syncytia by 48 hpi (Fig. 5A). BtCoV-422 also replicated in Vero-DPP4-KO cells in the presence of trypsin, albeit with reduced titers (about 10^4 PFU/mL at 48 hpi) (Fig. 5A and 5B) and reduced GFP and nLuc expression (Fig. 5A and 5C). These data support the hypothesis that BtCoV-422 has the potential to use a DPP4-independent pathway for Vero cell entry, but only in the presence of trypsin. In contrast, addition of trypsin during MERS-CoV infection caused extensive syncytia formation that resulted in a roughly 2-log decrease in viral yield (10^5 PFU/mL) as compared to no trypsin treatment (Fig. 5D and 5E). Additionally, MERS-CoV was unable to infect Vero-DPP4 KO cells even in the presence of trypsin, as supported by the lack of RFP and nLuc expression and lack of detectable virus growth (Fig. 5D to F).

BtCoV-422 spike protein does not bind to human ACE2 in vitro with high affinity.

As a recent report has shown a MERS-like CoV, NeoCoV, uses ACE2 as receptor, we used biolayer interferometry to assess the extent to which BtCoV-422 spike protein can bind to human ACE2. At the highest concentration of receptor tested (10 μM), we did not observe binding of immobilized BtCoV-422 spike protein to human ACE2. As expected, SARS-CoV-2 Omicron BA.1 spike protein bound ACE2 at 400 nM receptor concentration, but MERS-CoV spike protein did not (Fig. 5G). These results indicate that purified BtCoV-422 spike ectodomains do not have high affinity for soluble human ACE2.

Pan-sarbecovirus direct-acting antivirals (DAAs) inhibit MERS-CoV and BtCoV-422 replication.

BtCoV-422 and MERS-CoV share roughly 75% overall genome nucleotide identity. Individual proteins, such as the nsp12 RNA-dependent RNA polymerase (RdRp) and nsp5 main protease (M^{pro}), share 95% and 90% amino acid identity, but reduced identity (e.g., 88% and 56%) to SARS-CoV-2 RdRp and M^{pro} respectively (27, 28). To identify broadly cross protective merbecovirus countermeasures for use in future outbreaks, we evaluated a panel of inhibitors previously shown to be effective against MERS-CoV in other model systems, including the US Food and Drug Administration (FDA)-approved remdesivir (RDV) (29, 30), molnupiravir (EIDD-1931) (28), and the FDA-approved M^{pro} inhibitor nirmatrelvir (31, 32). All DAAs demonstrated potent antiviral activity against BtCoV-422 in vitro. The nucleoside analogue RDV and the M^{pro} inhibitor nirmatrelvir showed nanomolar potency against BtCoV-422 at 2.2 nM and 11.4 nM respectively (Fig. 6A). Molnupiravir, another nucleoside analogue, displayed a half-maximal inhibitory concentration (EC_{50}) of 0.388 μM (Fig. 6A). Together, these data indicate that FDA-authorized small-molecule inhibitors such as RDV and nirmatrelvir may prove useful (at nanomolar range) in the treatment of future group 2c outbreaks.

BtCoV-422 is neutralized by serum from mice vaccinated with a MERS-CoV mRNA and by the MERS-RBD antibody JC57–11.

To evaluate the antigenic relationships between BtCoV-422 and MERS-CoV, serum collected from mice vaccinated with different doses of a MERS-CoV mRNA vaccine (MERS-S2P) were tested against BtCoV-422. As previously reported, MERS-CoV vaccine-elicited serum potently neutralizes MERS-nLuc with a half-maximal inhibitory concentration (IC_{50}) of approximately 1:100 at medium doses (0.1μg/dose, 2 doses) and 1:1000 at high doses(33). We observed neutralization of BtCoV-422, although neutralization were 5- to 10-fold less potent than those observed for MERS-CoV (Fig. 6B). Given the moderate neutralization potency of MERS-CoV vaccine-elicited polyclonal serum against BtCoV-422, we hypothesized the likely existence of a small subset of broadly neutralizing monoclonal antibodies (mAbs) against a heterogeneous set of MERS-related viruses. To address this hypothesis, we evaluated a panel of neutralizing mAbs previously found to target the N terminal domain (NTD), RBD, or S2 domain of MERS-CoV (34, 35). Although all these antibodies demonstrated a range of neutralization titers against MERS-CoV as previously reported (34, 35), most displayed little if any neutralization against BtCoV-422 (Fig. 6C). However, a single MERS-CoV RBD-targeting mAb, JC57–11, was able to potently neutralize both BtCoV-422 and MERS-CoV (Fig. 6C). Importantly, the IC_{50} of JC57–11 against BtCoV-422 was 5.4 ng/ml, ~10-fold more potent than the IC_{50} against MERS-CoV (63 ng/ml) (Fig. 6C). Like antibodies targeting sarbecovirus RBDs, these data show that a small subset of MERS-CoV-targeting mAbs, such as JC57–11, have neutralizing properties against other antigenically distinct MERS-related virus RBD domains and are candidates for further development as broad countermeasures against multiple group 2c CoVs.

JC57–11 binds the RBD primarily through its long CDRH3.

To understand JC57–11's mechanism of neutralization, we determined a 3.0 Å resolution cryo-electron microscopy (EM) structure of the JC57–11 antigen-binding fragment (Fab) bound to the BtCoV-422 spike protein extracellular domain (Fig. 7A). To improve the quality of the map at the binding interface, local refinement was performed, resulting in a focused 3D reconstruction with a resolution of 3.1 Å (fig. S4). JC57–11 binds BtCoV-422 RBD exclusively through heavy chain interactions, predominately involving the third complementarity-determining region (CDRH3). Comprising 21 amino acids, the CDRH3 folds into a β-hairpin stabilized by a disulfide bond between Cys100 and Cys100E (Kabat numbering). This β-hairpin forms intermolecular anti-parallel β-sheet-like hydrogen bonds with a β-strand in the RBD composed of residues 542 to 548. Mainchain and sidechain atoms of RBD residue Thr546 interact with mainchain atoms of Cys100E, whereas the sidechain of RBD residue Asp543 forms a hydrogen bond with the sidechain of Tyr100F (Fig. 7B, left). Outside of the CDRH3, CDRH2 residue Thr53 forms a sidechain-sidechain hydrogen bond with RBD residue Tyr544. Collectively, JC57–11 interacts with two conserved residues shown to be involved in the MERS-CoV RBD-DPP4 binding interface: Asp543 and Tyr544 (Asp539 and Tyr540 in MERS-CoV spike protein). In MERS-CoV spike protein, Asp539 is part of a negatively charged patch that has been identified as critical for DPP4 binding and forms a salt bridge directly with Lys267 of DPP4 (36). Therefore, the mechanism of neutralization of JC57–11 involves occlusion of the DPP4 binding site.

An N-linked glycan on Asn170 within the NTD of the neighboring protomer of BtCoV-422 spike protein contributes 223 $Å^2$ of the total 840 $Å^2$ of surface area that is buried by JC57–11 (Fig. 7B, right). This glycosylation site is conserved in most merbecoviruses including MERS-CoV, BtCoV-HKU4, and BtCoV-HKU5 (fig. S5). Although the epitope of JC57–11 is accessible in both the RBD 'up' and 'down' conformations, the glycan on Asn170 is only proximal to the CDRH3 in the RBD-down conformation, suggesting that JC57–11 may bind with higher affinity to RBDs in the down conformation.

BtCoV-422 showed minor signs of viral replication in humanized 288/330$^{+/+}$ mice.

Given the rich genetically modified rodents and immunologic tools available, they are an important laboratory model for antiviral and vaccine testing. We attempted to develop an in vivo small animal model for BtCoV-422, using established MERS-CoV models. These include the 288/330$^{+/+}$ model, which mutations A288K and T330R in mouse (m) DPP4 restore a key hydrophobic interaction between MERS-RBD and mDPP4 and removes steric hindrance from an N-linked glycan (25);the 288/330$^{+/+}$-IFNαβγR KO, which has additional knockout of the type I and type II Interferon receptors, and the T330R model has the T330R mutation only(23). Inoculation of a non-mouse adapted BtCoV-422 was unable to establish a robust infection in any of the mouse models tested, either by physiological outcomes such as weight loss, or by virological indications such as lung titers (fig. S6A to C). However, signs of limited sub-genomic RNA transcription could be detected in infected animals, suggesting limited replication in vivo (fig. S6D). Similar evidence for inefficient replication of group 2c bat coronavirus has been reported in mice previously (19).

Discussion

The COVID-19 pandemic has resulted in over 6.8 million deaths and enormous economic losses globally, prompting concerns of a potential conversion of the ongoing MERS-CoV outbreak into a full-scale pandemic. Direct ancestral zoonotic virus precursors for camel and human MERS-CoV strains are still lacking but are thought to have originated in eastern Africa, most likely in bats (37). Given the vast number of MERS-like viruses in the bat population, current knowledge about the emergence potential of zoonotic merbecoviruses and reagents for testing broadly effective countermeasures are limited. Multiple MERS-like CoVs circulate through Asia, Africa, and Europe and use human DPP4 as receptors, providing clear support for the One Health Threat potential of these betacoronaviruses (13, 14, 19, 20, 38). However, no published study has shown replication in primary human airway cultures, although several MERS-related coronaviruses, such as *Tylonycteris* bat CoV HKU4 and *Pipistrellus* bat CoV HKU5 have been isolated (19, 20). Methods for successful high titer cultivation inevitably has required addition of exogenous proteases for improved in vitro growth or expression of cellular receptors for functional entry (19, 20). Initially isolated from the anal swab of the great evening bat (*Ia io*) in 2014, BtCoV-422 is a South East Asian relative of MERS-CoV (19, 38). The main habitat of *Ia Io* spreads from the southwestern part of China around Yunnan province to Southeast Asia including Nepal, Thailand, Vietnam, Myanmar, and Laos, in regions which contain high densities of human populations. Given the high virulence of MERS-CoV, a richer, well-characterized group 2c CoV panel is needed for the development and testing of broadly effective countermeasures and global preparedness.

Based on published sequences (14), we recovered a wild-type BtCoV-422 recombinant virus and two reporter viruses, BtCoV-422-GFP and BtCoV-422-nLuc, using reverse genetics. The synthetic recovery of a single, targeted wildtype virus from published full length RNAseq datasets at BSL3 (a single isolate among many in a sample) is inherently safer than traditional untargeted culture-based approaches using pooled specimens derived from multiple sources, oftentimes under BSL2 conditions (39–42). BtCoV-422 replicated efficiently in primary human non-ciliated distal airway cells such as LAEs, as well as MVEs and fibroblast cells, but replicated less efficiently than MERS-CoV in primary proximal human airway cells derived from the nasal epithelia of a subset of donors. BtCoV-422 growth correlated with the differential expression of DPP4 in the upper (URT) and lower respiratory tract (LRT) in the lung. DPP4 is highly expressed in type I and type II pneumocytes, and on non-ciliated bronchial epithelial cells in the LRT; however, DPP4 expression in the upper airway and nasal epithelium is more variable, potentially explaining sporadic transmission patterns (18, 43). BtCoV-422 replication in cells of the distal airway indicates its potential for cross-species transmission, although its reduced replication efficiency in the proximal airway may hinder transmission within human populations. For example, during the COVID-19 pandemic, a number of VOCs caused multiple waves of uncontrolled transmission, which was associated with more efficient replication in nasal epithelial cells (44, 45). We observed variation in susceptibility to viral infection between donors, particularly in NE cultures, in which donor 4 was completely resistant to MERS-CoV infection. This discrepancy may be due to a combination of genetic

variation and primary culture establishment. However, such differences do not affect our conclusion as the same donors were used in both MERS-CoV and BtCoV-422 infection.

In addition to its potential to infect humans, BtCoV-422 shows the potential to infect different animals based on its receptor usage. BtCoV-422 can utilize human, camel, and bat DPP4s as functional receptors, supporting earlier observations using pseudotyped viruses (14). Given high mutation and recombination rates, a stepwise adaptation of BtCoV-422 by mutation or recombination-driven evolution in an intermediate host is a possible pathway for human emergence. Like MERS-CoV, BtCoV-422 cannot use the mouse, hamster, guinea pig, or ferret DPP4s as functional receptors (26), most likely because glycans block DPP4 receptor usage in these species, but not in humans (25, 26). Despite using three different mouse models, inoculation of a non-mouse adapted BtCoV-422 demonstrated limited replication. Similar findings were reported with the self-limiting infection of BtCoV-HKU4 in a hDPP4 transgenic mouse model (19). Recently, a distant pangolin-CoV, MjHKU4r-CoV-1 showed efficient replication and pathology in the lung and brain in hDPP4 transgenic mice(15).

Viruses use host proteases to activate fusion proteins for spatiotemporal control of infection both in vitro and in vivo. For instance, influenza and CoV infections of the upper and lower respiratory tract use transmembrane serine protease 2(TMPRSS2) with or without other respiratory tract-expressed trypsin-like-proteases (48, 49). In addition, many avian influenza viruses and coronaviruses use a ubiquitously expressed furin protease for entry, potentially expanding virus tropism to other tissues (50, 51). Similarly, MERS-CoV and BtCoV-422 demonstrated enhanced infectivity and altered growth phenotype in the presence of external proteases, such as trypsin and elastase. This enhancement is likely due to the efficient processing of spike protein and the increased cell-to-cell spread by syncytia formation. Although the trypsin-mediated enhancement of infectivity of MERS-CoV was completely dependent on DPP4, BtCoV-422 appears to utilize an unknown, trypsin-dependent, DPP4-independent pathway to gain entry to the cells. Trypsin may act directly on spike protein or indirectly through other cryptic host receptors, but based on biolayer interferometry studies, BtCoV-422 does not bind the human ACE2 receptor (21). Alternatively, a recently identified host protein, placenta associated 8 (PLAC8), functions as an early replication factor for SADS-CoV infection (52) and several cofactors have been identified that enhance SARS-CoV-2, MERS-CoV and seasonal hCoV entry (53, 54). Such an alternative entry pathway might reflect “in transition viral adaptation” and could correlate with zoonotic transmission. The protease dependence of BtCoV-422 enables a host-targeting antiviral strategy.

There are currently no approved therapies to treat Merbecovirus infection. To address this, we evaluated the current arsenal of broad-spectrum CoV DAAs against BtCoV-422. Previous studies have demonstrated the antiviral potency of remdesivir and molnupiravir against SARS-CoV-2 both in vitro and in vivo (28–30), eventually leading to FDA authorization and clinical use (28). These two RdRp-targeting DAAs potently inhibit a broad array of coronaviruses, including MERS-CoV in vitro and in mouse models of human disease (28, 29). Remdesivir showed better efficacy than molnupiravir in suppressing BtCoV-422 in cell culture, demonstrating potential use of this drug in current and future MERS-like infections. In parallel, the FDA-approved SARS-CoV-2 M^{pro} inhibitor

Nirmatrelvir also showed nanomolar potency against BtCoV-422, despite encoding a heterogeneous nsp5 M^{pro}. Together, these data support the hypothesis that these drugs should be evaluated in the context of early treatments for MERS-CoV infection, which would provide potential high-performance drugs that could be used to treat humans experiencing novel Sarbecovirus and Merbecovirus infections.

Antigenically, BtCoV-422 is distantly related to MERS-CoV, but MERS-CoV mRNA vaccine serum was shown to be effective, albeit with reduced neutralization potency. Given the antigenic distance between these strains and the threat of BtCoV-422, these data argue for its use in future pan-merbecovirus and pan-betacoronavirus cocktail mRNA vaccines, chimeric mRNAs, or chimeric nanoparticles, as such formulations have shown robust protection in preclinical pan-sarbecovirus vaccine testing (56–59). Importantly, the identification that JC57–11, an anti-MERS-CoV RBD antibody, could cross-neutralize BtCoV-422 provides support for pan-merbecovirus neutralizing epitopes in the RBD, as reported among sarbecoviruses (60–62). In MERS-CoV, R540G, T412I, and S440A mutations on the lateral ridge of the RBD allow the virus to escape JC57–11 neutralization (34). Similarly, structural studies also reveal that JC57–11 binds to the lateral ridge of the RBD of BtCoV-422. Interestingly, JC57–11 has a lower affinity to BtCoV-422-RBD than to MERS-CoV-RBD, which is directly opposite to the different potencies of neutralization recorded between the two viruses. This difference could be due to the ratio between the up- and down-conformations of the RBDs in the spike proteins or other long-range mechanisms that regulate epitope presentation. Nevertheless, the neutralizing potency of JC57–11 against both MERS-CoV and BtCoV-422 supports its further development as a broadly protective therapeutic antibody and provides justification for additional discovery campaigns to identify broadly neutralizing epitopes and antibodies across the merbecoviruses.

Our study has limitations. Although we use primary airway cultures derived from multiple donors to account for genetic variations, the small sample size is not a representation of the population. The viruses used in this study are derived from reverse genetics, therefore minimizing the genetic variations present in natural isolates. Further, the lack of efficient BtCoV-422 replication in the rodent $288/330^{+/+}$hDPP4 model dictates the need for additional testing in other animal models of human disease.

In conclusion, our data indicates that BtCoV-422 has crossed multiple barriers that impede human emergence, such as infectivity in human cells. However, its reduced growth potential in the URT suggests that further mutation-driven evolution would be required for this virus to threaten human populations. Fortunately, multiple FDA-approved DAAs, as well as mAb JC57–11, showed inhibitory properties against BtCoV-422, providing therapeutic options ready for immediate testing. Finally, JC57–11 may represent the a potent, RBD-directed neutralizing antibody for multiple DPP4-utilizing group 2c coronaviruses.

Materials and Methods

Study Design

Our research objective was to understand the potential of BtCoV-422 in infecting clinically relevant human airway cultures and testing potential antivirals and antibodies against

BtCoV-422. Experiments were performed at least three independent times unless stated specifically in text due to limited reagents. For primary airway cultures, donor codes were matched to the best of our ability, and at least two individual donor codes were used for each experiment to account for genetic variation. Outliers (defined as documented experimental errors or 2-$\log_{10}$ from the mean) were excluded from the analysis in Fig. 6C (M336, CDC-C2, JC57–11, JC57–13, JC57–14 and G2).

Biosafety measures

Synthetic reconstruction of the authentic, wildtype BtCoV-422 virus was based on its published sequence(14) and undertaken with the approval of the Institutional Biosafety Committee of the University of North Carolina at Chapel Hill (approval 69349, approval date 12/5/2019). All constructs were handled under proper biosafety level conditions as specified by the institutional approval, with reconstructed live virus handled exclusively at biosafety level 3, with personnel wearing full-body personal protective equipment and HEPA-filtered respiratory protection. We note that "wild-type pathogens that are circulating in or have been recovered from nature are not enhanced PPPs, regardless of their pandemic potential" (https://www.phe.gov/s3/dualuse/Documents/P3CO-FinalGuidanceStatement.pdf).

Cells, plasmids, antibodies, and serum

Vero 81 cells [American Type Culture Collection (ATCC)# CCL-81), were maintain in in 5% CO_2 at 37°C incubator in Dulbecco's Modified Eagle Medium: Nutrient Mixture F-12 (DMEM/F12, Gibco) supplemented with 5% fetal bovine serum (FBS), 100 mg/mL penicillin/streptomycin (P/S, Gibco), 0.1 mM nonessential amino acids (NEAA), 0.075% sodium bicarbonate (Gibco), 0.01M HEPES and 2mM GlutaMax (Gibco). Huh7.5 cells (a gift from Dr. Charles M. Rice at The Rockefeller University and Apath, LLC) were maintained at 37°C + 5% CO_2 incubator in DMEM (high glucose, Gibco) supplemented with 10% FBS, 100 mg/mL P/S and 0.1 mM NEAA. Anti-MERS-CoV antibodies were kindly provided by Dr. Lingshu Wang and Dr. John Mascola at the Vaccine Research Center at NIH. For vaccine serum studies, mice received two doses of MERS-CoV-S2P mRNA vaccine (Moderna) at 1, 0.1 and 0.01 μg/mice at week 0 (prime) and week 3 (boost). Serum samples were collected 1 month after boost and were heat-inactivated at 56°C for 30 minutes prior to use.

Coronavirus reverse genetics

BtCoV-422 infectious clones were constructed from published wildtype sequence using a six-plasmid cloning strategy as described previously(64). A T7 promoter was introduced into the 5′ end, and ORF5 was replaced with either GFP or nLuc. Each fragment was flanked by a unique type IIS restriction endonuclease cleavage sites. Plasmids was restriction digested, gel purified, and ligated together with T4 DNA ligase (New England Biolabs). Ligation products were purified by chloroform extraction and used as a template for in vitro transcription with T7 RNA polymerase (Thermo Fisher Scientific). RNA was electroporated into Vero81 cells along with mRNA transcript encoding *BtCoV-422* N protein. Virus-containing supernatant was harvested 1 to 3 days post-electroporation and

subsequently passaged. The individual plasmid digestion steps were handled at BSL-2. Ligation of the full-length cDNA and all subsequent steps were performed at BSL-3.

Primary human airway cultures

The generation of primary human pulmonary cell cultures was described previously (65). Primary human NE cells, human bronchial epithelial (LAE) and bronchiolarcells were isolated from freshly excised normal human tissues obtained from transplant donors under UNC Institutional Review Board (IRB)-approved protocol (#03–1396) and cultured in air-liquid interface (ALI) media, as previously described (66). The age and gender of the donors included males and females at 21 to 70 years of age.

Whole-mount immunostaining and imaging of primary cells

Primary airway cell cultures were fixed twice for 30 minutes in 4% formaldehyde in phosphate-buffered saline (PBS) and washed and stored in PBS. The viral signals were stained by mouse antiserum against MERS-CoV N protein (1:500 dilution) using species-specific secondary antibodies as previously described. The human NE and LAE cultures were also imaged for a-tubulin (Millipore MAB1864; 3μg/mL), MUC5AC (Thermo Fisher Scientific 45M1; 4μg/mL), MUC5B [polyclonal rabbit against a MUC5B peptide (MAN5BII), (UNC222) 1:1000](67), and Club Cell Secretory Protein (CCSP) (Sigma 07–623; 1:2000) as indicated. Filamentous actin was localized with phalloidin (Invitrogen A22287), and DNA with Hoechst 33342 (Invitrogen). An Olympus FV3000RS confocal microscope in Galvo scan mode was used to acquire 5-channel Z stacks by the 2-phase sequential scan. Representative stacks were acquired with a 60X oil objective (XYZ = 212μm x 212μm x about 25μm) and shown as Z-projections or single-slice, XZ cross-sections to distinguish individual cell features to characterize the infected cell types. A 20X objective was used to acquire 2D, single-channel, apical snapshots of nine fields (636μm x 636μm; combined area = 3.64mm^2), selected in evenly spaced grids across each sham infected donor culture, and ImageJ was used to measure the relative apical culture surface covered by multiciliated cells.

CRISPR-KO cell line and stable cell line generation

Vero 81 DPP4 KO cells were generated by CRISPR/Cas9 as described previously using the lentiCRIPRv2 system (Addgene #98290) (68). KO cells were under blasticidin (20 μg/ml) selection and subsequently clonally selected by limited dilution. Clonal CRISPR KO cells were sequence confirmed by Sanger sequencing. DPP4 from multiple species were cloned in the sleeping beauty transposon plasmid pSB-bi-RP (Addgene #60513) and transfected along with transposase, pCMV(CAT)T7-SB100 (Addgene #34879), into Vero 81 DPP4 KO cells using lipofectamine 3000 (Invitrogen) and selected with 10 μg/mL Puromycin (Gibco). Clonal cell lines were generated through limited dilution(69, 70).

Virus growth kinetics and plaque assays

WT or DPP4-KO Vero cells were infected with either BtCoV-422-GFP or MERS-RFP and were cultured in the present or absent of exogenous trypsin. Supernatants were collected at different timepoints and were titrated using plaque assay. For BtCoV-422 plaque assays,

monolayer of Vero cells were infected with serially diluted virus for 1h, then covered with agarose overlays with 10 μg/mL trypsin. At 2 days post infection, infected cells were stained with neutral red solution. The plaque assay for MERS-CoV were performed similarly with no addition of trypsin in the agarose overlays.

nLuc virus protease entry assay

Monolayers of Caco-2, Calu 3, and Vero cells were cultured in black-walled 96-well plates (Corning 3904) overnight. The cells were infected with BtCoV-422-nLuc at a multiplicity of infection (MOI) of 0.02 in the presence of different proteases. After incubation at 37°C for 24h, viral entry was quantified by measuring nLuc activity using Nano-Glo Luciferase Assay System (Promega) according to the manufacturer's specifications.

Protein expression and purification

Plasmids encoding JC57–11 heavy chain and light chain were previously described (34). The heavy chain was modified to include an HRV3C protease cleavage site between the CH1 and CH2 regions for facile digestion of IgG to Fab. A codon-optimized gene encoding the ectodomain of the BtCoV-422 spike protein, MERS-CoV spike protein, SARS-CoV-2 Omicron BA.1 spike protein, and human ACE2 was cloned into the mammalian expression vector paH upstream of a C-terminal foldon trimerization motif from T4 fibritin (71), an HRV3C protease cleavage site, an 8X His tag, and a Twin-Strep tag. Three proline substitutions were introduced to stabilize BtCoV-422 spike protein at positions 885, 1056, and 1057. (72)

Spikes proteins, hACE2 or JC57–11 IgG plasmids (1:1 ratio) were transiently transfected into FreeStyle293F cells (Thermo Fisher Scientific) using 25 kDa linear polyethylenimine (PEI), with 5 μM kifunensine added 3h post-transfection. Cultures were grown for 6 days, and culture supernatant was separated by centrifugation and passed through a 0.22 μm filter. Protein of BtCoV-422 spike, MERS-CoV spike, SARS-CoV-2 spike, and hACE2 were purified from supernatant using StrepTactin resin following the manufacturer's instructions (IBA). Purified hACE2 was treated with HRV3C protease for 2 hours at room temperature to remove affinity tags from the C terminus. JC57–11 Fab was purified by flowing IgG-containing supernatant over a Protein A column (Pierce), incubating the resin with HRV3C protease at 4 °C overnight, and collecting the eluent. Proteins were further purified by size-exclusion chromatography using a HiLoad 16/600 Superdex 200 pg for spike proteins or Superdex 200 Increase 10/300 GL column for JC57–11 Fab and hACE2 (GE Healthcare) in a buffer composed of 2 mM Tris pH 8.0, 200 mM NaCl and 0.02% NaN_3. Purified proteins were concentrated, flash frozen, and stored at −80°C.

Biolayer interferometry

Purified MERS-CoV, SARS-CoV-2 Omicron BA.1, and BtCoV-422 spike proteins were immobilized on streptavidin biosensors that were pre-soaked in buffer consisting of 10 mM HEPES pH 7.4, 150 mM NaCl, 3 mM EDTA, 0.05% Surfactant P20, and 1% bovine serum albumin. Biosensors loaded with spike proteins were dipped into buffer for 60 seconds to measure baseline signal and subsequently dipped into 400 nM or 10 μM purified ACE2 to

measure the binding response for 180 seconds. The response from a biosensor that was not loaded with spike proteins but dipped into human ACE2 was used for reference subtraction.

Cryo-EM

BtCoV-422 spike protein was incubated with a 3-fold molar excess of JC57–11 Fab in 2 mM Tris pH 8.0, 200 mM NaCl and 0.02% NaN_3 and brought to a final concentration of 2 mg/mL with PBS. Sample was incubated on ice for 2 minutes and then deposited on a plasma-cleaned CF-400 1.2/1.3 grid before being blotted for 3 s with −3 force in a Vitrobot Mark IV (Thermo Fisher Scientific) and plunge-frozen into liquid ethane. 2,666 micrographs were collected from a single grid on a FEI Titan Krios (Thermo Fisher Scientific) equipped with a K3 direct electron detector (Gatan). The microscope was operated with an accelerating voltage of 300 kV and a total electron flux of 80.5 e^{-}/A^2. Data were collected at a magnification of 105,000X, corresponding to a calibrated pixel size of 0.83 Å/pix. A full description of the data collection parameters can be found in table S1. CryoSPARC v4.0.1 (73, 74) was used for data processing, which includes patch-based motion correction, patch-based contrast transfer function (CTF) estimation, particle picking, and then curation of the particles through iterative rounds of 2D classification. 3D volumes were generated using ab initio reconstruction, and data were further processed through heterogeneous refinement, homogenous refinement, and subsequently non-uniform homogeneous refinement of final classes. A representative processing workflow can be found in fig. S7. To achieve higher resolution in the Fab–RBD interface, local refinement was performed with masks made in ChimeraX (75). The structure validation can be found in table S1. Models were docked into the experimental EM maps using ChimeraX and further refined by Phenix (76), *Coot* (77), and ISOLDE (78). The starting homology model for BtCoV-422 spike protein was constructed by SWISS-MODEL (79). For JC57–11 Fab, an initial homology model was generated using the SAbPred server (80).

Neutralization Assay of BtCoV-*422*-nLuc and MERS-CoV-nLuc

Neutralization on Huh7.5 cell were performed as described previously(52). In brief, Huh7.5 cells were seeded in at Day −1 on a black-well, black-wall, tissue culture treated, 96-well plate (Corning Cat. #3916) at 2×10^4 cells/well. mAbs were diluted in DMEM supplemented with 5% FBS and 1% P/S to obtain an 8-point, 3-fold dilution curve with starting concentration at various starting concentration, from 20 to 160 μg/ml. Eight hundred PFU of BtCoV-422-nLuc and MERS-CoV-nLuc viruses were mixed with mAbs at a 1:1 ratio and incubated at 37°C for 1 h. One-hundred microliters of virus and mAb mix was added to each well and incubated at 37°C + 5% CO_2 for 20 to 22 h. Luciferase activity was measured by the Nano-Glo Luciferase Assay System (Promega Cat. #N1130) following the manufacturer's protocol using a GloMax luminometer (Promega). Percent inhibition and IC_{50} were calculated by the following equation: % Neutralization = [(RLU of no Ab or serum – RLU of Sample)/(Average RLU of no Ab or Serum)] x100%. All experiments were performed as duplicate and independently repeated three times.

Antiviral Assay of BtCoV-422-nLuc

The antiviral activity of RDV, molnupiravir, and nirmatrelvir against BtCoV-*422* was measured in a Huh7.5 cell line-based assay. Huh7.5 cells were maintained in DMEM

(Gibco), 20% FBS and 1X Antibiotic-Antimycotic (A.A., Gibco). Twenty-four hours after plating 2×10^4 cells/well, fresh medium was added. In triplicate, cells were exposed to serial dilutions of drug (RDV, molnupiravir, nirmatrelvir) or vehicle (DMSO) in "infection medium" (similar to that above but with 5% FBS) and immediately infected for 1 h with BtCoV-422-nLuc added at 800 PFU/well. Virus was then removed, and cells were rinsed once, and infection medium containing dilutions of drug or vehicle was added. At 24 hours post infection, virus replication was measured by nLuc assay (Promega Cat. #N1130) and then read on a Promega GloMax luminometer (Promega) following manufacturer's instructions. The IC_{50} value was defined in Graphpad Prism 9.0 (GraphPad) as the concentration at which there was a 50% decrease in viral replication using non-infected wells (100% inhibition) and infected and vehicle-treated wells (0% inhibition) as controls.

In vivo infection of BtCoV-422 in mouse models

$288/330^{+/+}$ hDDP4, T330R, and $288/330^{+/+}$-IFNαβγR knock-out mice were bred at the University of North Carolina at Chapel Hill. Ten- to 36-week-old female and male mice were randomly assigned to experimental groups and transferred into the BSL3 seven days prior to virus infection to acclimate. At the day of infection, mice were anesthetized with a mixture of Ketamine and Xylazine and then intranasally infected with indicated concentrations of virus diluted in PBS to a final volume of 50μl. Changes in body weight, as a measure for clinical signs of disease, were monitored daily until the end of the experiment 4 days after infection. Mice were euthanized by isoflurane overdose. Caudal right lung lobes were collected and transferred into tubes containing glass beads in 1mL of PBS and stored at −80°C until further processing. To determine viral loads, lung samples were thawed, homogenized, and centrifuged. Lung homogenate supernatants were used to perform plaque assays as described above. To determine viral replication, total RNA samples were extracted from the lung tissue and were subjected to amplification of subgenomic RNAs by RT-PCR. Briefly, the total RNA was extracted from lung tissue using Trizol reagent (Invitrogen), and the cDNA was generated using SuperScript reverse transcription kit (Invitrogen). The subgenomic RNA flanking the leader sequence and partial 5'-end region of the nucleocapsid gene was amplified using forward primer TTAAGTGAATAGCCCAGCTAGCTC and reverse primer CTGTTGCACCATCTTCGTGGAC. All experiments were approved by the Institutional Animal Care and Use Committee at UNC Chapel Hill (animal protocol number: 19–206) according to guidelines outlined by the Association for the Assessment and Accreditation of Laboratory Animal Care and the U.S. Department of Agriculture.

Statistical analysis

All raw, individual-level data for experiments where n<20 is presented in data file S1. Error bar represents ± 1 SD. Data in Fig. 3C and 3D were analyzed using one-way ANOVA compared with Vero-KO values. Data in Fig. 4A, 4B and 4C were analyzed using one-way ANOVA compared with values in the No Protease group. Data in Fig. 5C and 5F were analyzed using non-parametric t-test compared with the corresponding background values. Statistical analysis was carried out using GraphPad Prism version 9.0. Significance symbols are defined as follow: *p<0.05, **p< 0.01, ***p<0.001, ****p<0.0001. Data are graphed as mean ± standard deviation.

Supplementary Material

Refer to Web version on PubMed Central for supplementary material.

Acknowledgments

Funding:

This work was supported by NIAID AVIDD AI171292, AI151797, AI116484, and AI158571, and R01 AI132178 grants (to R.S.B). D.R.M. is funded by a Burroughs Wellcome Fund Postdoctoral Enrichment Program Award and a Hanna H. Gray Fellowship from the Howard Hughes Medical Institute. The work was also supported by NIH NIAID R01-AI127521 and a Welch Foundation grant F-0003-19620604 (to J.S.M.)

Data and materials availability:

All data associated with this study are in the paper or supplementary materials. Atomic coordinates and cryo-EM maps of the reported structure have been deposited in the Protein Data Bank under accession code 8SAK and in the Electron Microscopy Data Bank under accession codes EMD-40272 (composite map), EMD-40306 (global map), and EMD-40310 (local refinement map). Plasmids associated with Cryo-EM data are available from J.S.M. under a material transfer agreement with The University of Texas at Austin. Plasmids used in the study are available from R.S.B. under a standard material transfer agreement with The University of North Carolina at Chapel Hill. In parallel, BtCoV-422 wildtype and derivative reporter viruses will be made available through BEI (https://www.beiresources.org/).

References

1. Zhou P, Yang X-L, Wang X-G, Hu B, Zhang L, Zhang W, Si H-R, Zhu Y, Li B, Huang C-L, Chen H-D, Chen J, Luo Y, Guo H, Jiang R-D, Liu M-Q, Chen Y, Shen X-R, Wang X, Zheng X-S, Zhao K, Chen Q-J, Deng F, Liu L-L, Yan B, Zhan F-X, Wang Y-Y, Xiao G-F, Shi Z-L, A pneumonia outbreak associated with a new coronavirus of probable bat origin. Nature (2020), doi:10.1038/s41586-020-2012-7.
2. Updates on COVID-19 Variants of Concern (VOC).
3. Zaki AM, van Boheemen S, Bestebroer TM, Osterhaus ADME, Fouchier RAM, Isolation of a Novel Coronavirus from a Man with Pneumonia in Saudi Arabia. New England Journal of Medicine. 367, 1814–1820 (2012). [PubMed: 23075143]
4. Baric RS, Sullivan E, Hensley L, Yount B, Chen W, Persistent Infection Promotes Cross-Species Transmissibility of Mouse Hepatitis Virus. J Virol. 73, 638 (1999). [PubMed: 9847369]
5. Arabi YM, Arifi AA, Balkhy HH, Najm H, Aldawood AS, Ghabashi A, Hawa H, Alothman A, Khaldi A, al Raiy B, Clinical course and outcomes of critically ill patients with Middle East respiratory syndrome coronavirus infection. Ann Intern Med. 160, 389–397 (2014). [PubMed: 24474051]
6. Killerby ME, Biggs HM, Midgley CM, Gerber SI, Watson JT, Middle East Respiratory Syndrome Coronavirus Transmission. Emerg Infect Dis. 26, 191 (2020). [PubMed: 31961300]
7. Zhang AR, Shi WQ, Liu K, lou Li X, Liu MJ, Zhang WH, Zhao GP, Chen JJ, Zhang XA, Miao D, Ma W, Liu W, Yang Y, Fang LQ, Epidemiology and evolution of Middle East respiratory syndrome coronavirus, 2012–2020. Infect Dis Poverty. 10, 1–13 (2021). [PubMed: 33397494]
8. Zhou P, Fan H, Lan T, lou Yang X, Shi WF, Zhang W, Zhu Y, Zhang YW, Xie QM, Mani S, Zheng XS, Li B, Li JM, Guo H, Pei GQ, An XP, Chen JW, Zhou L, Mai KJ, Wu ZX, Li D, Anderson DE, Zhang LB, Li SY, Mi ZQ, He TT, Cong F, Guo PJ, Huang R, Luo Y, Liu XL, Chen J, Huang Y, Sun Q, Zhang XLL, Wang YY, Xing SZ, Chen YS, Sun Y, Li J, Daszak P, Wang LF, Shi ZL, Tong YG, Ma JY, Fatal swine acute diarrhoea syndrome caused by an HKU2-related coronavirus of bat origin. Nature. 556, 255–259 (2018). [PubMed: 29618817]

9. Huang YW, Dickerman AW, Piñeyro P, Li L, Fang L, Kiehne R, Opriessnig T, Meng XJ, Origin, evolution, and genotyping of emergent porcine epidemic diarrhea virus strains in the united states. mBio. 4, 737–750 (2013).
10. Huynh J, Li S, Yount B, Smith A, Sturges L, Olsen JC, Nagel J, Johnson JB, Agnihothram S, Gates JE, Frieman MB, Baric RS, Donaldson EF, Evidence Supporting a Zoonotic Origin of Human Coronavirus Strain NL63. J Virol. 86, 12816–12825 (2012). [PubMed: 22993147]
11. Corman VM, Baldwin HJ, Tateno AF, Zerbinati RM, Annan A, Owusu M, Nkrumah EE, Maganga GD, Oppong S, Adu-Sarkodie Y, Vallo P, da Silva Filho LVRF, Leroy EM, Thiel V, van der Hoek L, Poon LLM, Tschapka M, Drosten C, Drexler JF, Evidence for an Ancestral Association of Human Coronavirus 229E with Bats. J Virol. 89, 11858–11870 (2015). [PubMed: 26378164]
12. Brüssow H, Brüssow L, Clinical evidence that the pandemic from 1889 to 1891 commonly called the Russian flu might have been an earlier coronavirus pandemic. Microb Biotechnol. 14, 1860–1870 (2021). [PubMed: 34254725]
13. Lau SKP, Li KSM, Tsang AKL, Lam CSF, Ahmed S, Chen H, Chan K-H, Woo PCY, Yuen K-Y, Genetic characterization of Betacoronavirus lineage C viruses in bats reveals marked sequence divergence in the spike protein of pipistrellus bat coronavirus HKU5 in Japanese pipistrelle: implications for the origin of the novel Middle East respiratory syndrome coronavirus. J Virol. 87, 8638–8650 (2013). [PubMed: 23720729]
14. Luo C-M, Wang N, Yang X-L, Liu H-Z, Zhang W, Li B, Hu B, Peng C, Geng Q-B, Zhu G-J, Li F, Shi Z-L, Discovery of Novel Bat Coronaviruses in South China That Use the Same Receptor as Middle East Respiratory Syndrome Coronavirus. J Virol. 92 (2018), doi:10.1128/JVI.00116-18.
15. Chen J, Yang X, Si H, Gong Q, Que T, Li J, Li Y, Wu C, Zhang W, Chen Y, Luo Y, Zhu Y, Li B, Luo D, Hu B, Lin H, Jiang R, Jiang T, Li Q, Liu M, Xie S, Su J, Zheng X, Li A, Yao Y, Yang Y, Chen P, Wu A, He M, Lin X, Tong Y, Hu Y, Shi ZL, Zhou P, A bat MERS-like coronavirus circulates in pangolins and utilizes human DPP4 and host proteases for cell entry. Cell. 186, 850–863.e16 (2023). [PubMed: 36803605]
16. Millet JK, Whittaker GR, Host cell entry of Middle East respiratory syndrome coronavirus after two-step, furin-mediated activation of the spike protein. Proc Natl Acad Sci U S A. 111, 15214–15219 (2014). [PubMed: 25288733]
17. van Doremalen N, Miazgowicz KL, Milne-Price S, Bushmaker T, Robertson S, Scott D, Kinne J, McLellan JS, Zhu J, Munster VJ, Host Species Restriction of Middle East Respiratory Syndrome Coronavirus through Its Receptor, Dipeptidyl Peptidase 4. J Virol. 88, 9220 (2014). [PubMed: 24899185]
18. Raj VS, Mou H, Smits SL, Dekkers DHW, Müller MA, Dijkman R, Muth D, Demmers JAA, Zaki A, Fouchier RAM, Thiel V, Drosten C, Rottier PJM, Osterhaus ADME, Bosch BJ, Haagmans BL, Dipeptidyl peptidase 4 is a functional receptor for the emerging human coronavirus-EMC. Nature. 495, 251 (2013). [PubMed: 23486063]
19. Lau SKP, Fan RYY, Zhu L, Li KSM, Wong ACP, Luk HKH, Wong EYM, Lam CSF, Lo GCS, Fung J, He Z, Fok FCH, Au-Yeung RKH, Zhang L, Kok KH, Yuen KY, Woo PCY, Isolation of MERS-related coronavirus from lesser bamboo bats that uses DPP4 and infects human-DPP4-transgenic mice. Nature Communications 2021 12:1. 12, 1–10 (2021).
20. Menachery VD, Dinnon KH, Yount BL, McAnarney ET, Gralinski LE, Hale A, Graham RL, Scobey T, Anthony SJ, Wang L, Graham B, Randell SH, Lipkin WI, Baric RS, Trypsin Treatment Unlocks Barrier for Zoonotic Bat Coronavirus Infection. J Virol. 94 (2020), doi:10.1128/JVI.01774-19/ASSET/EF17A1B2-3456-4BDB-9B2E-8BB16AECC307/ASSETS/GRAPHIC/JVI.01774-19-F0007.JPEG.
21. Xiong Q, Cao L, Ma C, Tortorici MA, Liu C, Si J, Liu P, Gu M, Walls AC, Wang C, Shi L, Tong F, Huang M, Li J, Zhao C, Shen C, Chen Y, Zhao H, Lan K, Corti D, Veesler D, Wang X, Yan H, Close relatives of MERS-CoV in bats use ACE2 as their functional receptors. Nature 2022, 1–10 (2022).
22. Moreno A, Lelli D, de Sabato L, Zaccaria G, Boni A, Sozzi E, Prosperi A, Lavazza A, Cella E, Castrucci MR, Cicozzi M, Vaccari G, Detection and full genome characterization of two beta CoV viruses related to Middle East respiratory syndrome from bats in Italy. Virol J. 14 (2017), doi:10.1186/S12985-017-0907-1.

23. Scobey T, Yount BL, Sims AC, Donaldson EF, Agnihothram SS, Menachery VD, Graham RL, Swanstrom J, Bove PF, Kim JD, Grego S, Randell SH, Baric RS, Reverse genetics with a full-length infectious cDNA of the Middle East respiratory syndrome coronavirus. Proceedings of the National Academy of Sciences. 110, 16157–16162 (2013).
24. Sims AC, Mitchell HD, Gralinski LE, Kyle JE, Burnum-Johnson KE, Lam M, Fulcher ML, West A, Smith RD, Randell SH, Metz TO, Sheahan TP, Waters KM, Baric RS, Unfolded Protein Response Inhibition Reduces Middle East Respiratory Syndrome Coronavirus-Induced Acute Lung Injury. mBio. 12 (2021), doi:10.1128/MBIO.01572-21.
25. Peck KM, Cockrell AS, Yount BL, Scobey T, Baric RS, Heise MT, Glycosylation of mouse DPP4 plays a role in inhibiting Middle East respiratory syndrome coronavirus infection. J Virol. 89, 4696–4699 (2015). [PubMed: 25653445]
26. Peck KM, Scobey T, Swanstrom J, Jensen KL, Burch CL, Baric RS, Heise MT, Permissivity of Dipeptidyl Peptidase 4 Orthologs to Middle East Respiratory Syndrome Coronavirus Is Governed by Glycosylation and Other Complex Determinants. J Virol. 91 (2017), doi:10.1128/JVI.00534-17.
27. Yang KS, Leeuwon SZ, Xu S, Liu WR, Evolutionary and Structural Insights about Potential SARS-CoV-2 Evasion of Nirmatrelvir. J Med Chem. 65, 8686–8698 (2022). [PubMed: 35731933]
28. Sheahan TP, Sims AC, Zhou S, Graham RL, Pruijssers AJ, Agostini ML, Leist SR, Schafer A, Dinnon KH, Stevens LJ, Chappell JD, Lu X, Hughes TM, George AS, Hill CS, Montgomery SA, Brown AJ, Bluemling GR, Natchus MG, Saindane M, Kolykhalov AA, Painter G, Harcourt J, Tamin A, Thornburg NJ, Swanstrom R, Denison MR, Baric RS, An orally bioavailable broad-spectrum antiviral inhibits SARS-CoV-2 in human airway epithelial cell cultures and multiple coronaviruses in mice. Sci Transl Med. 12, 5883 (2020).
29. Sheahan TP, Sims AC, Graham RL, Menachery VD, Gralinski LE, Case JB, Leist SR, Pyrc K, Feng JY, Trantcheva I, Bannister R, Park Y, Babusis D, Clarke MO, MacKman RL, Spahn JE, Palmiotti CA, Siegel D, Ray AS, Cihlar T, Jordan R, Denison MR, Baric RS, Broad-spectrum antiviral GS-5734 inhibits both epidemic and zoonotic coronaviruses. Sci Transl Med. 9 (2017), doi:10.1126/SCITRANSLMED.AAL3653.
30. Sheahan TP, Sims AC, Leist SR, Schäfer A, Won J, Brown AJ, Montgomery SA, Hogg A, Babusis D, Clarke MO, Spahn JE, Bauer L, Sellers S, Porter D, Feng JY, Cihlar T, Jordan R, Denison MR, Baric RS, Comparative therapeutic efficacy of remdesivir and combination lopinavir, ritonavir, and interferon beta against MERS-CoV. Nature Communications 2020 11:1. 11, 1–14 (2020).
31. Kim Y, Liu H, Galasiti Kankanamalage AC, Weerasekara S, Hua DH, Groutas WC, Chang KO, Pedersen NC, Reversal of the Progression of Fatal Coronavirus Infection in Cats by a Broad-Spectrum Coronavirus Protease Inhibitor. PLoS Pathog. 12 (2016), doi:10.1371/JOURNAL.PPAT.1005531.
32. Sacco MD, Ma C, Lagarias P, Gao A, Townsend JA, Meng X, Dube P, Zhang X, Hu Y, Kitamura N, Hurst B, Tarbet B, Marty MT, Kolocouris A, Xiang Y, Chen Y, Wang J, Structure and inhibition of the SARS-CoV-2 main protease reveal strategy for developing dual inhibitors against Mpro and cathepsin L. Sci Adv. 6 (2020), doi:10.1126/SCIADV.ABE0751/SUPPL_FILE/ABE0751_SM.PDF.
33. Corbett KS, Edwards DK, Leist SR, Abiona OM, Boyoglu-Barnum S, Gillespie RA, Himansu S, Schäfer A, Ziwawo CT, DiPiazza AT, Dinnon KH, Elbashir SM, Shaw CA, Woods A, Fritch EJ, Martinez DR, Bock KW, Minai M, Nagata BM, Hutchinson GB, Wu K, Henry C, Bahl K, Garcia-Dominguez D, Ma LZ, Renzi I, Kong WP, Schmidt SD, Wang L, Zhang Y, Phung E, Chang LA, Loomis RJ, Altaras NE, Narayanan E, Metkar M, Presnyak V, Liu C, Louder MK, Shi W, Leung K, Yang ES, West A, Gully KL, Stevens LJ, Wang N, Wrapp D, Doria-Rose NA, Stewart-Jones G, Bennett H, Alvarado GS, Nason MC, Ruckwardt TJ, McLellan JS, Denison MR, Chappell JD, Moore IN, Morabito KM, Mascola JR, Baric RS, Carfi A, Graham BS, SARS-CoV-2 mRNA Vaccine Design Enabled by Prototype Pathogen Preparedness. Nature. 586, 567 (2020). [PubMed: 32756549]
34. Wang L, Shi W, Chappell JD, Joyce MG, Zhang Y, Kanekiyo M, Becker MM, van Doremalen N, Fischer R, Wang N, Corbett KS, Choe M, Mason RD, van Galen JG, Zhou T, Saunders KO, Tatti KM, Haynes LM, Kwong PD, Modjarrad K, Kong W-P, McLellan JS, Denison MR, Munster VJ, Mascola JR, Graham BS, Importance of Neutralizing Monoclonal Antibodies Targeting Multiple

Antigenic Sites on the Middle East Respiratory Syndrome Coronavirus Spike Glycoprotein To Avoid Neutralization Escape. J Virol. 92 (2018), doi:10.1128/JVI.02002-17.

35. Wang L, Shi W, Joyce MG, Modjarrad K, Zhang Y, Leung K, Lees CR, Zhou T, Yassine HM, Kanekiyo M, Yang ZY, Chen X, Becker MM, Freeman M, Vogel L, Johnson JC, Olinger G, Todd JP, Bagci U, Solomon J, Mollura DJ, Hensley L, Jahrling P, Denison MR, Rao SS, Subbarao K, Kwong PD, Mascola JR, Kong WP, Graham BS, Evaluation of candidate vaccine approaches for MERS-CoV. Nature Communications 2015 6:1. 6, 1–11 (2015).
36. Wang N, Shi X, Jiang L, Zhang S, Wang D, Tong P, Guo D, Fu L, Cui Y, Liu X, Arledge KC, Chen YH, Zhang L, Wang X, Structure of MERS-CoV spike receptor-binding domain complexed with human receptor DPP4. Cell Res. 23, 986–993 (2013). [PubMed: 23835475]
37. Ithete NL, Stoffberg S, Corman VM, Cottontail VM, Richards LR, Schoeman MC, Drosten C, Drexler JF, Preiser W, Close Relative of Human Middle East Respiratory Syndrome Coronavirus in Bat, South Africa. Emerg Infect Dis. 19, 1697 (2013). [PubMed: 24050621]
38. Yang Y, Du L, Liu C, Wang L, Ma C, Tang J, Baric RS, Jiang S, Li F, Receptor usage and cell entry of bat coronavirus HKU4 provide insight into bat-to-human transmission of MERS coronavirus. Proc Natl Acad Sci U S A. 111, 12516–12521 (2014). [PubMed: 25114257]
39. Liu M-Q, Lin H-F, Li J, Chen Y, Luo Y, Zhang W, Hu B, Tian F-J, Hu Y-J, Liu Y-J, Jiang R-D, Gong Q-C, Li A, Guo Z-S, Li B, Yang X-L, Tong Y-G, Shi Z-L, A SARS-CoV-2-Related Virus from Malayan Pangolin Causes Lung Infection without Severe Disease in Human ACE2-Transgenic Mice. J Virol. 97 (2023), doi:10.1128/JVI.01719-22.
40. Eckerle I, Lenk M, Ulrich RG, More Novel Hantaviruses and Diversifying Reservoir Hosts — Time for Development of Reservoir-Derived Cell Culture Models? Viruses. 6, 951 (2014). [PubMed: 24576845]
41. Zeng L-P, Gao Y-T, Ge X-Y, Zhang Q, Peng C, Yang X-L, Tan B, Chen J, Chmura AA, Daszak P, Shi Z-L, Bat Severe Acute Respiratory Syndrome-Like Coronavirus WIV1 Encodes an Extra Accessory Protein, ORFX, Involved in Modulation of the Host Immune Response. J Virol. 90, 6573 (2016). [PubMed: 27170748]
42. Ge XY, Li JL, Lou Yang X, Chmura AA, Zhu G, Epstein JH, Mazet JK, Hu B, Zhang W, Peng C, Zhang YJ, Luo CM, Tan B, Wang N, Zhu Y, Crameri G, Zhang SY, Wang LF, Daszak P, Shi ZL, Isolation and characterization of a bat SARS-like coronavirus that uses the ACE2 receptor. Nature. 503, 535 (2013). [PubMed: 24172901]
43. Zumla A, Hui DS, Perlman S, Middle East respiratory syndrome. Lancet. 386, 995 (2015). [PubMed: 26049252]
44. Meng B, Abdullahi A, Ferreira IATM, Goonawardane N, Saito A, Kimura I, Yamasoba D, Gerber PP, Fatihi S, Rathore S, Zepeda SK, Papa G, Kemp SA, Ikeda T, Toyoda M, Tan TS, Kuramochi J, Mitsunaga S, Ueno T, Shirakawa K, Takaori-Kondo A, Brevini T, Mallery DL, Charles OJ, Baker S, Dougan G, Hess C, Kingston N, Lehner PJ, Lyons PA, Matheson NJ, Ouwehand WH, Saunders C, Summers C, Thaventhiran JED, Toshner M, Weekes MP, Maxwell P, Shaw A, Bucke A, Calder J, Canna L, Domingo J, Elmer A, Fuller S, Harris J, Hewitt S, Kennet J, Jose S, Kourampa J, Meadows A, O'Brien C, Price J, Publico C, Rastall R, Ribeiro C, Rowlands J, Ruffolo V, Tordesillas H, Bullman B, Dunmore BJ, Gräf S, Hodgson J, Huang C, Hunter K, Jones E, Legchenko E, Matara C, Martin J, Mescia F, O'Donnell C, Pointon L, Shih J, Sutcliffe R, Tilly T, Treacy C, Tong Z, Wood J, Wylot M, Betancourt A, Bower G, Cossetti C, de Sa A, Epping M, Fawke S, Gleadall N, Grenfell R, Hinch A, Jackson S, Jarvis I, Krishna B, Nice F, Omarjee O, Perera M, Potts M, Richoz N, Romashova V, Stefanucci L, Strezlecki M, Turner L, de Bie EMDD, Bunclark K, Josipovic M, Mackay M, Butcher H, Caputo D, Chandler M, Chinnery P, Clapham-Riley D, Dewhurst E, Fernandez C, Furlong A, Graves B, Gray J, Hein S, Ivers T, le Gresley E, Linger R, Kasanicki M, King R, Kingston N, Meloy S, Moulton A, Muldoon F, Ovington N, Papadia S, Penkett CJ, Phelan I, Ranganath V, Paraschiv R, Sage A, Sambrook J, Scholtes I, Schon K, Stark H, Stirrups KE, Townsend P, Walker N, Webster J, Butlertanaka EP, Tanaka YL, Ito J, Uriu K, Kosugi Y, Suganami M, Oide A, Yokoyama M, Chiba M, Motozono C, Nasser H, Shimizu R, Kitazato K, Hasebe H, Irie T, Nakagawa S, Wu J, Takahashi M, Fukuhara T, Shimizu K, Tsushima K, Kubo H, Kazuma Y, Nomura R, Horisawa Y, Nagata K, Kawai Y, Yanagida Y, Tashiro Y, Tokunaga K, Ozono S, Kawabata R, Morizako N, Sadamasu K, Asakura H, Nagashima M, Yoshimura K, Cárdenas P, Muñoz E, Barragan V, Márquez S, Prado-Vivar B, Becerra-Wong M, Caravajal M, Trueba G, Rojas-Silva P, Grunauer M, Gutierrez B, Guadalupe

JJ, Fernández-Cadena JC, Andrade-Molina D, Baldeon M, Pinos A, Bowen JE, Joshi A, Walls AC, Jackson L, Martin D, Smith KGC, Bradley J, Briggs JAG, Choi J, Madissoon E, Meyer KB, Mlcochova P, Ceron-Gutierrez L, Doffinger R, Teichmann SA, Fisher AJ, Pizzuto MS, de Marco A, Corti D, Hosmillo M, Lee JH, James LC, Thukral L, Veesler D, Sigal A, Sampaziotis F, Goodfellow IG, Matheson NJ, Sato K, Gupta RK, Altered TMPRSS2 usage by SARS-CoV-2 Omicron impacts infectivity and fusogenicity. Nature. 603, 706–714 (2022). [PubMed: 35104837]

45. Yamasoba D, Kimura I, Nasser H, Morioka Y, Nao N, Ito J, Uriu K, Tsuda M, Zahradnik J, Shirakawa K, Suzuki R, Kishimoto M, Kosugi Y, Kobiyama K, Hara T, Toyoda M, Tanaka YL, Butlertanaka EP, Shimizu R, Ito H, Wang L, Oda Y, Orba Y, Sasaki M, Nagata K, Yoshimatsu K, Asakura H, Nagashima M, Sadamasu K, Yoshimura K, Kuramochi J, Seki M, Fujiki R, Kaneda A, Shimada T, aki Nakada T, Sakao S, Suzuki T, Ueno T, Takaori-Kondo A, Ishii KJ, Schreiber G, Sawa H, Saito A, Irie T, Tanaka S, Matsuno K, Fukuhara T, Ikeda T, Sato K, Virological characteristics of the SARS-CoV-2 Omicron BA.2 spike. Cell. 185, 2103–2115.e19 (2022). [PubMed: 35568035]
46. Cockrell AS, Yount BL, Scobey T, Jensen K, Douglas M, Beall A, Tang XC, Marasco WA, Heise MT, Baric RS, A mouse model for MERS coronavirus-induced acute respiratory distress syndrome. Nature Microbiology 2016 2:2. 2, 1–11 (2016).
47. Douglas MG, Kocher JF, Scobey T, Baric RS, Cockrell AS, Adaptive evolution influences the infectious dose of MERS-CoV necessary to achieve severe respiratory disease. Virology. 517, 98–107 (2018). [PubMed: 29277291]
48. Böttcher E, Matrosovich T, Beyerle M, Klenk H-D, Garten W, Matrosovich M, Proteolytic Activation of Influenza Viruses by Serine Proteases TMPRSS2 and HAT from Human Airway Epithelium. J Virol. 80, 9896–9898 (2006). [PubMed: 16973594]
49. Hoffmann M, Kleine-Weber H, Schroeder S, Krüger N, Herrler T, Erichsen S, Schiergens TS, Herrler G, Wu NH, Nitsche A, Müller MA, Drosten C, Pöhlmann S, SARS-CoV-2 Cell Entry Depends on ACE2 and TMPRSS2 and Is Blocked by a Clinically Proven Protease Inhibitor. Cell. 181, 271–280.e8 (2020). [PubMed: 32142651]
50. Horimoto T, Nakayama K, Smeekens SP, Y. Kawaokal14, Proprotein-processing endoproteases PC6 and furin both activate hemagglutinin of virulent avian influenza viruses. J Virol. 68, 6074–6078 (1994). [PubMed: 8057485]
51. Stieneke-Grober A, Vey M, Angliker H, Shaw E, Thomas G, Roberts C, Klenk HD, Garten W, Influenza virus hemagglutinin with multibasic cleavage site is activated by furin, a subtilisin-like endoprotease. EMBO J. 11, 2407–2414 (1992). [PubMed: 1628614]
52. v Tse L, Meganck RM, Araba KC, Yount BL, Shaffer KM, Hou YJ, Munt JE, Adams LE, Wykoff JA, Morowitz JM, Dong S, Magness ST, Marzluff WF, Gonzalez LM, Ehre C, Baric RS, Genomewide CRISPR knockout screen identified PLAC8 as an essential factor for SADS-CoVs infection. Proc Natl Acad Sci U S A. 119, e2118126119 (2022). [PubMed: 35476513]
53. Peng R, Wu LA, Wang Q, Qi J, Gao GF, Cell entry by SARS-CoV-2. Trends Biochem Sci. 46, 848–860 (2021). [PubMed: 34187722]
54. Rebendenne A, Roy P, Bonaventure B, Chaves Valadão AL, Desmarets L, Arnaud-Arnould M, Rouillé Y, Tauziet M, Giovannini D, Touhami J, Lee Y, DeWeirdt P, Hegde M, Urbach S, el Koulali K, de Gracia FG, McKellar J, Dubuisson J, Wencker M, Belouzard S, Moncorgé O, Doench JG, Goujon C, Bidirectional genome-wide CRISPR screens reveal host factors regulating SARS-CoV-2, MERS-CoV and seasonal HCoVs. Nature Genetics 2022 54:8. 54, 1090–1102 (2022).
55. Cho SY, Kang JM, Ha YE, Park GE, Lee JY, Ko JH, Lee JY, Kim JM, Kang CI, Jo IJ, Ryu JG, Choi JR, Kim S, Huh HJ, Ki CS, Kang ES, Peck KR, Dhong HJ, Song JH, Chung DR, Kim YJ, MERS-CoV outbreak following a single patient exposure in an emergency room in South Korea: an epidemiological outbreak study. Lancet. 388, 994–1001 (2016). [PubMed: 27402381]
56. Walls AC, Fiala B, Schäfer A, Wrenn S, Pham MN, Murphy M, v Tse L, Shehata L, O'Connor MA, Chen C, Navarro MJ, Miranda MC, Pettie D, Ravichandran R, Kraft JC, Ogohara C, Palser A, Chalk S, Lee E-C, Guerriero K, Kepl E, Chow CM, Sydeman C, Hodge EA, Brown B, Fuller JT, Dinnon KH 3rd, Gralinski LE, Leist SR, Gully KL, Lewis TB, Guttman M, Chu HY, Lee KK, Fuller DH, Baric RS, Kellam P, Carter L, Pepper M, Sheahan TP, Veesler D, King NP,

Elicitation of Potent Neutralizing Antibody Responses by Designed Protein Nanoparticle Vaccines for SARS-CoV-2. Cell. 183, 1367–1382.e17 (2020). [PubMed: 33160446]

57. Saunders KO, Lee E, Parks R, Martinez DR, Li D, Chen H, Edwards RJ, Gobeil S, Barr M, Mansouri K, Alam SM, Sutherland LL, Cai F, Sanzone AM, Berry M, Manne K, Bock KW, Minai M, Nagata BM, Kapingidza AB, Azoitei M, Tse L. v., Scobey TD, Spreng RL, Rountree RW, DeMarco CT, Denny TN, Woods CW, Petzold EW, Tang J, Oguin TH, Sempowski GD, Gagne M, Douek DC, Tomai MA, Fox CB, Seder R, Wiehe K, Weissman D, Pardi N, Golding H, Khurana S, Acharya P, Andersen H, Lewis MG, Moore IN, Montefiori DC, Baric RS, Haynes BF, Neutralizing antibody vaccine for pandemic and pre-emergent coronaviruses. Nature 2021 594:7864. 594, 553–559 (2021).
58. Li D, Martinez DR, Schäfer A, Chen H, Barr M, Sutherland LL, Lee E, Parks R, Mielke D, Edwards W, Newman A, Bock KW, Minai M, Nagata BM, Gagne M, Douek DC, DeMarco CT, Denny TN, Oguin TH, Brown A, Rountree W, Wang Y, Mansouri K, Edwards RJ, Ferrari G, Sempowski GD, Eaton A, Tang J, Cain DW, Santra S, Pardi N, Weissman D, Tomai MA, Fox CB, Moore IN, Andersen H, Lewis MG, Golding H, Seder R, Khurana S, Baric RS, Montefiori DC, Saunders KO, Haynes BF, Breadth of SARS-CoV-2 neutralization and protection induced by a nanoparticle vaccine. Nature Communications 2022 13:1. 13, 1–15 (2022).
59. Martinez DR, Schäfer A, Leist SR, de la Cruz G, West A, Atochina-Vasserman EN, Lindesmith LC, Pardi N, Parks R, Barr M, Li D, Yount B, Saunders KO, Weissman D, Haynes BF, Montgomery SA, Baric RS, Chimeric spike mRNA vaccines protect against Sarbecovirus challenge in mice. Science. 373, 991–998 (2021). [PubMed: 34214046]
60. Rappazzo CG, v Tse L, Kaku CI, Wrapp D, Sakharkar M, Huang D, Deveau LM, Yockachonis TJ, Herbert AS, Battles MB, O'Brien CM, Brown ME, Geoghegan JC, Belk J, Peng L, Yang L, Hou Y, Scobey TD, Burton DR, Nemazee D, Dye JM, Voss JE, Gunn BM, McLellan JS, Baric RS, Gralinski LE, Walker LM, Broad and potent activity against SARS-like viruses by an engineered human monoclonal antibody. Science. 371, 823–829 (2021). [PubMed: 33495307]
61. ting He W, Musharrafieh R, Song G, Dueker K, Tse L. v., Martinez DR, Schäfer A, Callaghan S, Yong P, Beutler N, Torres JL, Volk RM, Zhou P, Yuan M, Liu H, Anzanello F, Capozzola T, Parren M, Garcia E, Rawlings SA, Smith DM, Wilson IA, Safonova Y, Ward AB, Rogers TF, Baric RS, Gralinski LE, Burton DR, Andrabi R, Targeted isolation of diverse human protective broadly neutralizing antibodies against SARS-like viruses. Nature Immunology 2022 23:6. 23, 960–970 (2022).
62. Martinez DR, Schäfer A, Gobeil S, Li D, de la Cruz G, Parks R, Lu X, Barr M, Stalls V, Janowska K, Beaudoin E, Manne K, Mansouri K, Edwards RJ, Cronin K, Yount B, Anasti K, Montgomery SA, Tang J, Golding H, Shen S, Zhou T, Kwong PD, Graham BS, Mascola JR, Montefiori DC, Alam SM, Sempowski GD, Khurana S, Wiehe K, Saunders KO, Acharya P, Haynes BF, Baric RS, A broadly cross-reactive antibody neutralizes and protects against sarbecovirus challenge in mice. Sci Transl Med. 14 (2022), doi:10.1126/SCITRANSLMED.ABJ7125.
63. Agnihothram S, Yount BL, Donaldson EF, Huynh J, Menachery VD, Gralinski LE, Graham RL, Becker MM, Tomar S, Scobey TD, Osswald HL, Whitmore A, Gopal R, Ghosh AK, Mesecar A, Zambon M, Heise M, Denison MR, Baric RS, A Mouse Model for Betacoronavirus Subgroup 2c Using a Bat Coronavirus Strain HKU5 Variant. mBio. 5 (2014), doi:10.1128/MBIO.00047-14.
64. Hou YJ, Chiba S, Halfmann P, Ehre C, Kuroda M, Dinnon KH 3rd, Leist SR, Schäfer A, Nakajima N, Takahashi K, Lee RE, Mascenik TM, Graham R, Edwards CE, v Tse L, Okuda K, Markmann AJ, Bartelt L, de Silva A, Margolis DM, Boucher RC, Randell SH, Suzuki T, Gralinski LE, Kawaoka Y, Baric RS, SARS-CoV-2 D614G variant exhibits efficient replication ex vivo and transmission in vivo. Science (2020), doi:10.1126/science.abe8499.
65. Hou YJ, Okuda K, Edwards CE, Martinez DR, Asakura T, Dinnon KH, Kato T, Lee RE, Yount BL, Mascenik TM, Chen G, Olivier KN, Ghio A, Tse L. v., Leist SR, Gralinski LE, Schäfer A, Dang H, Gilmore R, Nakano S, Sun L, Fulcher ML, Livraghi-Butrico A, Nicely NI, Cameron M, Cameron C, Kelvin DJ, de Silva A, Margolis DM, Markmann A, Bartelt L, Zumwalt R, Martinez FJ, Salvatore SP, Borczuk A, Tata PR, Sontake V, Kimple A, Jaspers I, O'Neal WK, Randell SH, Boucher RC, Baric RS, SARS-CoV-2 Reverse Genetics Reveals a Variable Infection Gradient in the Respiratory Tract. Cell. 182, 429 (2020). [PubMed: 32526206]
66. Fulcher ML, Randell SH, Human nasal and tracheo-bronchial respiratory epithelial cell culture. Methods Mol Biol. 945, 109–121 (2013). [PubMed: 23097104]

67. Ehre C, Worthington EN, Liesman RM, Grubb BR, Barbier D, O'Neal WK, Sallenave JM, Pickles RJ, Boucher RC, Overexpressing mouse model demonstrates the protective role of Muc5ac in the lungs. Proc Natl Acad Sci U S A. 109, 16528–16533 (2012). [PubMed: 23012413]
68. Sanjana NE, Shalem O, Zhang F, Improved vectors and genome-wide libraries for CRISPR screening. Nat Methods. 11, 783 (2014). [PubMed: 25075903]
69. Kowarz E, Löscher D, Marschalek R, Optimized Sleeping Beauty transposons rapidly generate stable transgenic cell lines. Biotechnol. J, 647–653 (2015). [PubMed: 25650551]
70. V Tse L, Meganck RM, Dong S, Adams LE, White LJ, Mallory ML, Jadi R, de Silva AM, Baric RS, Generation of Mature DENVs via Genetic Modification and Directed Evolution. mBio, e0038622 (2022). [PubMed: 35481749]
71. Efimov VP, Nepluev I. v., Sobolev BN, Zurabishvili TG, Schulthess T, Lustig A, Engel J, Haener M, Aebi U, Venyaminov SY, Potekhin SA, Mesyanzhinov V. v., Fibritin encoded by bacteriophage T4 gene wac has a parallel triple-stranded α-helical coiled-coil structure. J Mol Biol. 242, 470–486 (1994). [PubMed: 7932704]
72. Pallesen J, Wang N, Corbett KS, Wrapp D, Kirchdoerfer RN, Turner HL, Cottrell CA, Becker MM, Wang L, Shi W, Kong W-P, Andres EL, Kettenbach AN, Denison MR, Chappell JD, Graham BS, Ward AB, McLellan JS, Immunogenicity and structures of a rationally designed prefusion MERS-CoV spike antigen. Proc Natl Acad Sci U S A. 114, E7348–E7357 (2017). [PubMed: 28807998]
73. Punjani A, Zhang H, Fleet DJ, Non-uniform refinement: adaptive regularization improves single-particle cryo-EM reconstruction. Nat Methods. 17, 1214–1221 (2020). [PubMed: 33257830]
74. Punjani A, Rubinstein JL, Fleet DJ, Brubaker MA, cryoSPARC: algorithms for rapid unsupervised cryo-EM structure determination. Nat Methods. 14, 290–296 (2017). [PubMed: 28165473]
75. Pettersen EF, Goddard TD, Huang CC, Meng EC, Couch GS, Croll TI, Morris JH, Ferrin TE, UCSF ChimeraX: Structure visualization for researchers, educators, and developers. Protein Sci. 30, 70–82 (2021). [PubMed: 32881101]
76. Liebschner D, Afonine P. v., Baker ML, Bunkoczi G, Chen VB, Croll TI, Hintze B, Hung LW, Jain S, McCoy AJ, Moriarty NW, Oeffner RD, Poon BK, Prisant MG, Read RJ, Richardson JS, Richardson DC, Sammito MD, Sobolev O. v., Stockwell DH, Terwilliger TC, Urzhumtsev AG, Videau LL, Williams CJ, Adams PD, Macromolecular structure determination using X-rays, neutrons and electrons: recent developments in Phenix. Acta Crystallogr D Struct Biol. 75, 861–877 (2019). [PubMed: 31588918]
77. Emsley P, Lohkamp B, Scott WG, Cowtan K, Features and development of Coot. Acta Crystallogr D Biol Crystallogr. 66, 486–501 (2010). [PubMed: 20383002]
78. Croll TI, ISOLDE: a physically realistic environment for model building into low-resolution electron-density maps. Acta Crystallogr D Struct Biol. 74, 519–530 (2018). [PubMed: 29872003]
79. Waterhouse A, Bertoni M, Bienert S, Studer G, Tauriello G, Gumienny R, Heer FT, de Beer TAP, Rempfer C, Bordoli L, Lepore R, Schwede T, SWISS-MODEL: homology modelling of protein structures and complexes. Nucleic Acids Res. 46, W296–W303 (2018). [PubMed: 29788355]
80. Abanades B, Georges G, Bujotzek A, Deane CM, ABlooper: fast accurate antibody CDR loop structure prediction with accuracy estimation. Bioinformatics. 38, 1877–1880 (2022). [PubMed: 35099535]

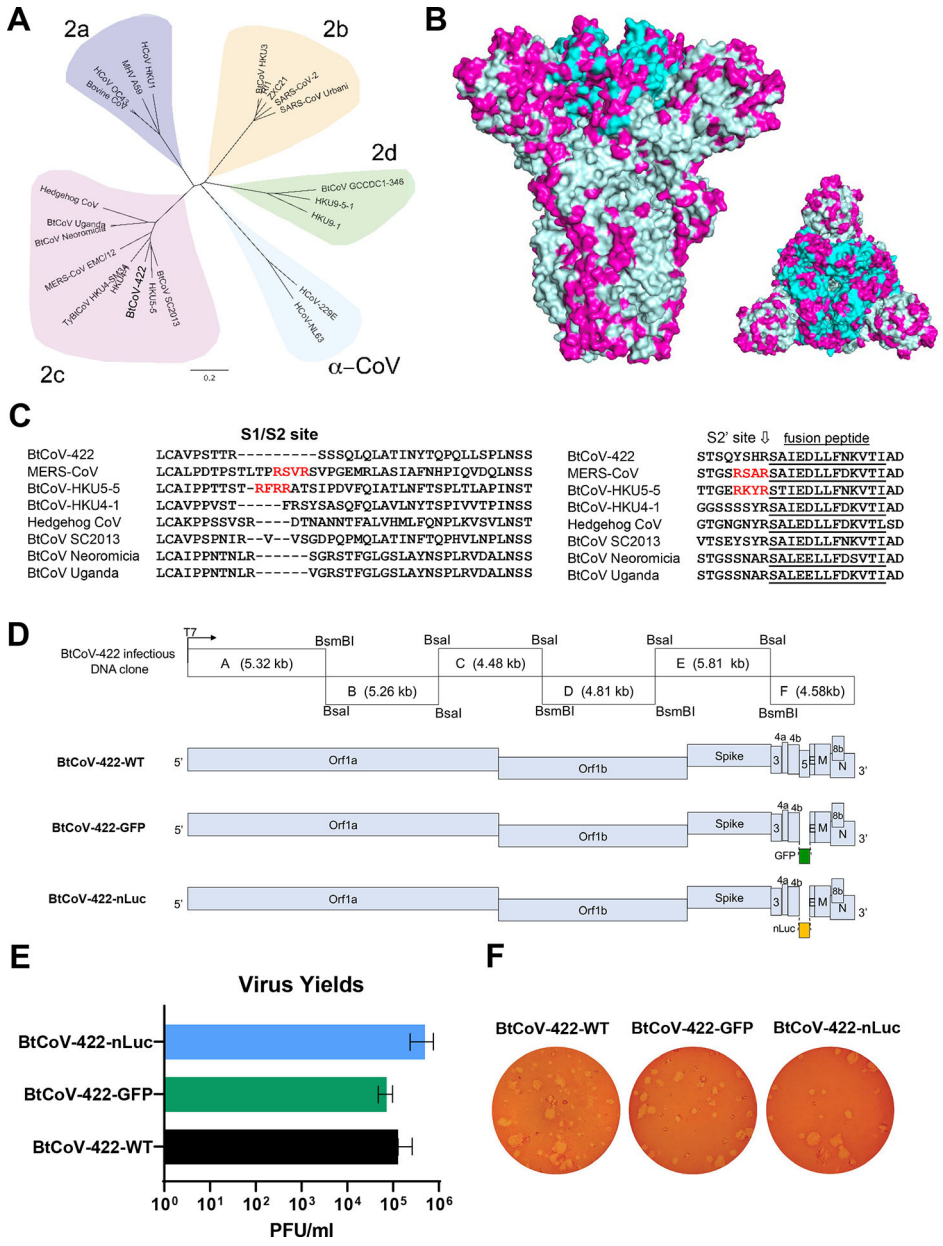

Figure 1. BtCoV-422 recombinant and reporter viruses were generated using reverse genetics.

(**A**) Shown is a phylogenetic tree of coronavirus spike proteins. (**B**) Structural alignment of spike proteins is shown for the indicated viruses. Magenta denotes amino acid variations and cyan denotes the RDB of spike protein. (**C**) Shown are the putative proteolytic cleavage sites in S1/S2 site and S2' site in multiple group 2C CoVs, including BtCoV-422 and MERS-CoV. The red text indicates furin cleavage sites. The underlined text indicates fusion peptides. (**D**) Shown is the design of BtCoV-422 infectious clones, including the wildtype clone, BtCoV-422-WT, the GFP reporter virus, BtCoV-422-GFP, and the nLuc reporter virus, BtCoV-422-nLuc. The size of each fragment, the restriction sites for cloning and the T7 promoter are shown. (**E**) Viral yields are shown for the BtCoV-422-WT virus and

reporter viruses. The data are presented as mean ± SD. **(F)** Plaque morphologies are shown for BtCoV-422-WT and reporter viruses on Vero cells stained with neutral red.

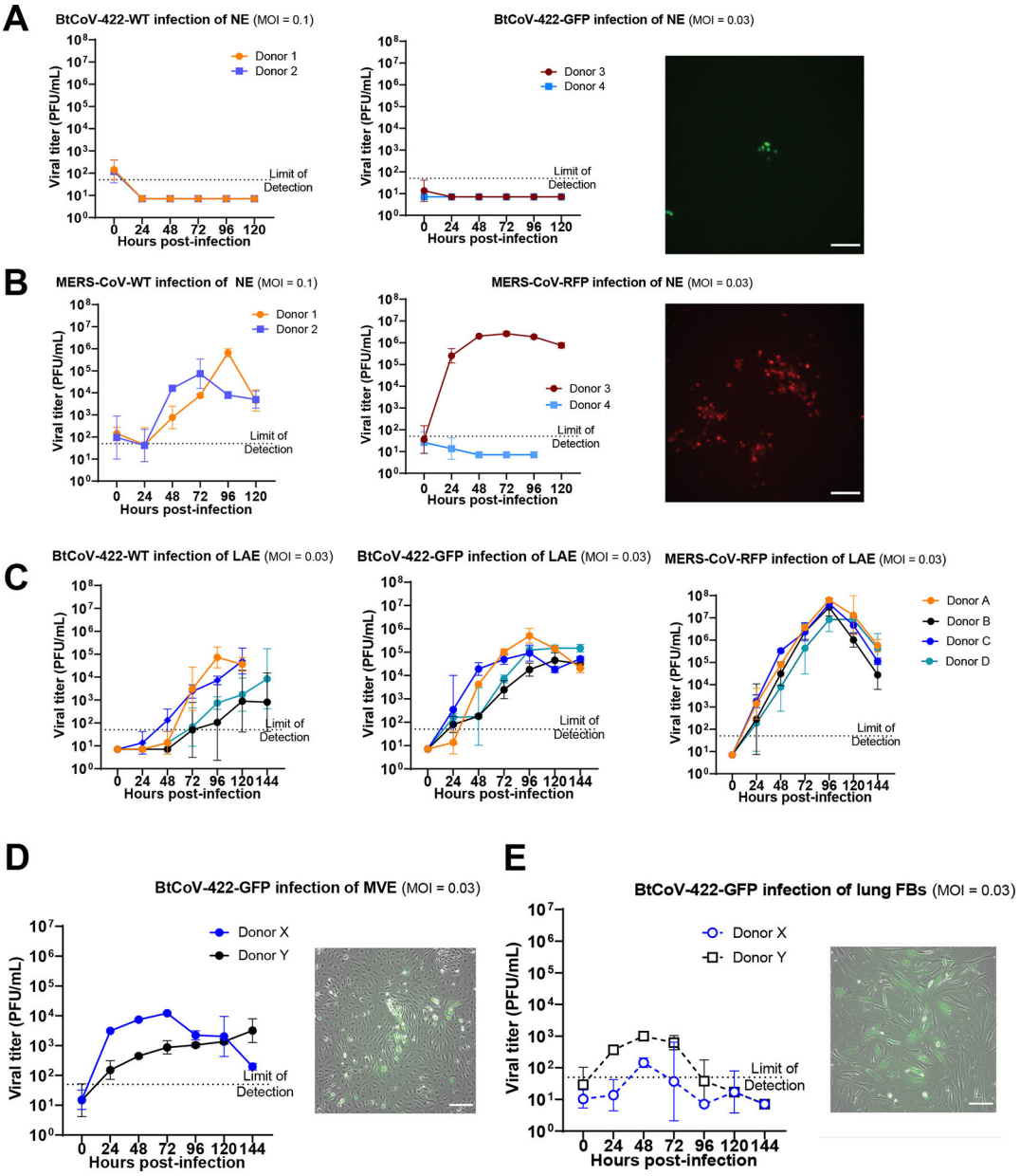

Figure 2. BtCoV-422 infects distal but not proximal primary human airway epithelial cultures.

(**A**) Shown are viral growth kinetics and representative fluorescent images of primary human nasal epithelial cells (NEs) from 4 different donors infected with BtCoV-422 or BtCoV-422-GFP. (**B**) Shown are viral growth kinetics and representative fluorescent images of primary human NEs from 4 different donors infected with MERS-CoV or MERS-CoV-RFP. Scale bars indicate 200 μm. (**C**) Shown are viral growth kinetics of BtCoV-422, BtCoV-422-GFP, and MERS-CoV-RFP in LAEs from 4 different donors. (D and E) Shown are growth kinetics and representative fluorescent images of BtCoV-422-GFP in primary human microvascular endothelial cells (MVEs) (**D**) and primary human lung fibroblasts (FBs) (E). Scale bars indicate 200 μm. The data are presented as mean ± SD.

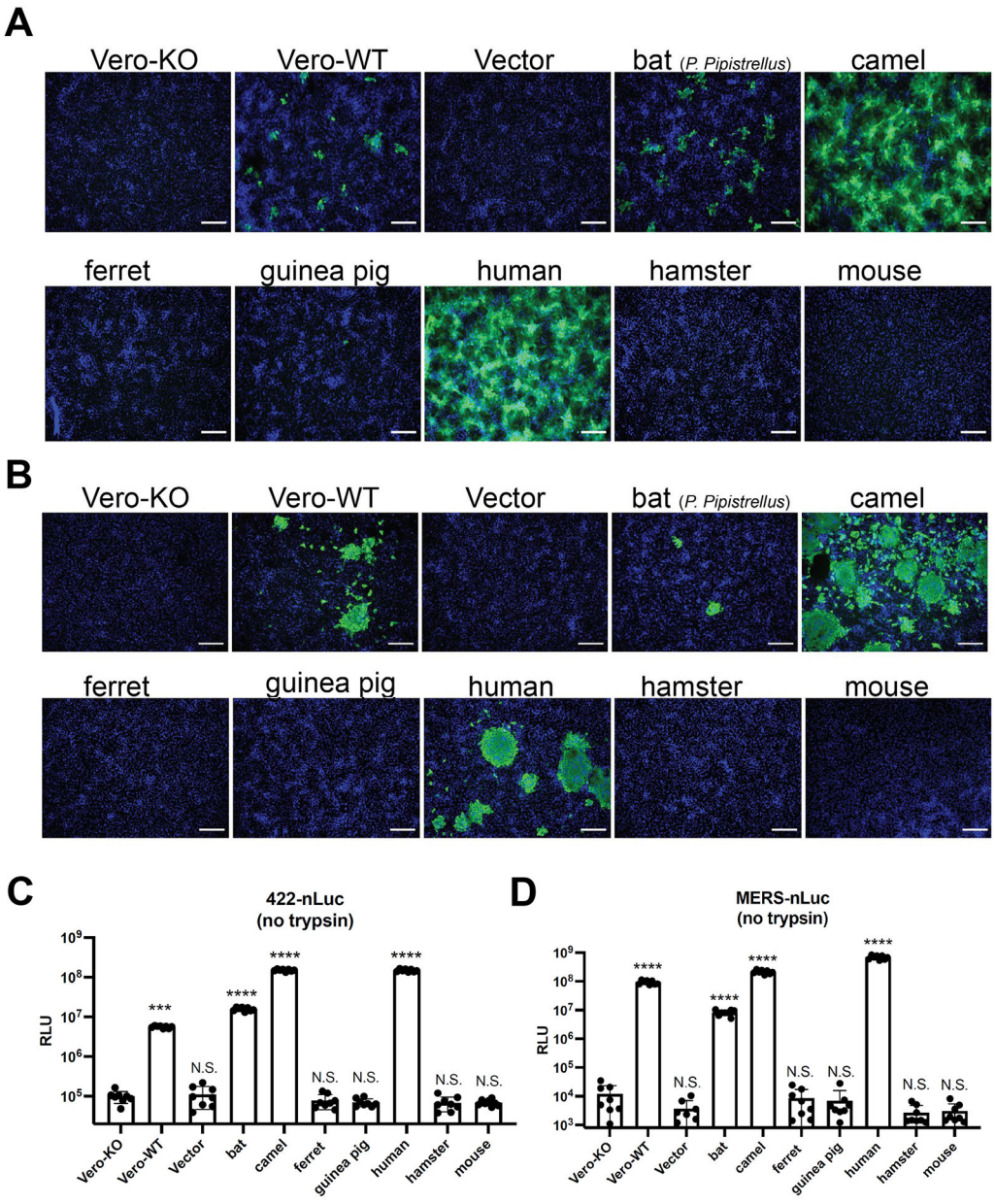

Figure 3. BtCoV-422 and MERS-CoV use similar species profile of DPP4 as functional receptors.

(**A and B**) Shown are representative images of BtCoV-422 (A) and MERS-CoV (B) infection of Vero-DPP4 KO cells, Vero-DPP4 WT cells, and Vero-DPP4 KO cells stably expressing a panel of seven DPP4 orthologs from other species, including bat *(P. Pipistrellus)*, camel, ferret, guinea pig, human, hamster, and mouse. Vector control is also shown. Infected cells were stained with anti-N antibodies. The scale bars indicate 200 μm. (**C and D**) Shown is quantitative analysis of BtCoV-422-nLuc (C) and MERS-CoV-nLuc (D) infecting the same panel of DPP4 cell lines. Relative light units (RLUs) were compared using one-way ANOVA to DPP4-KO cells. N.S., not significant; ***P < 0.001; ****P < 0.0001. The data are presented as mean ± SD.

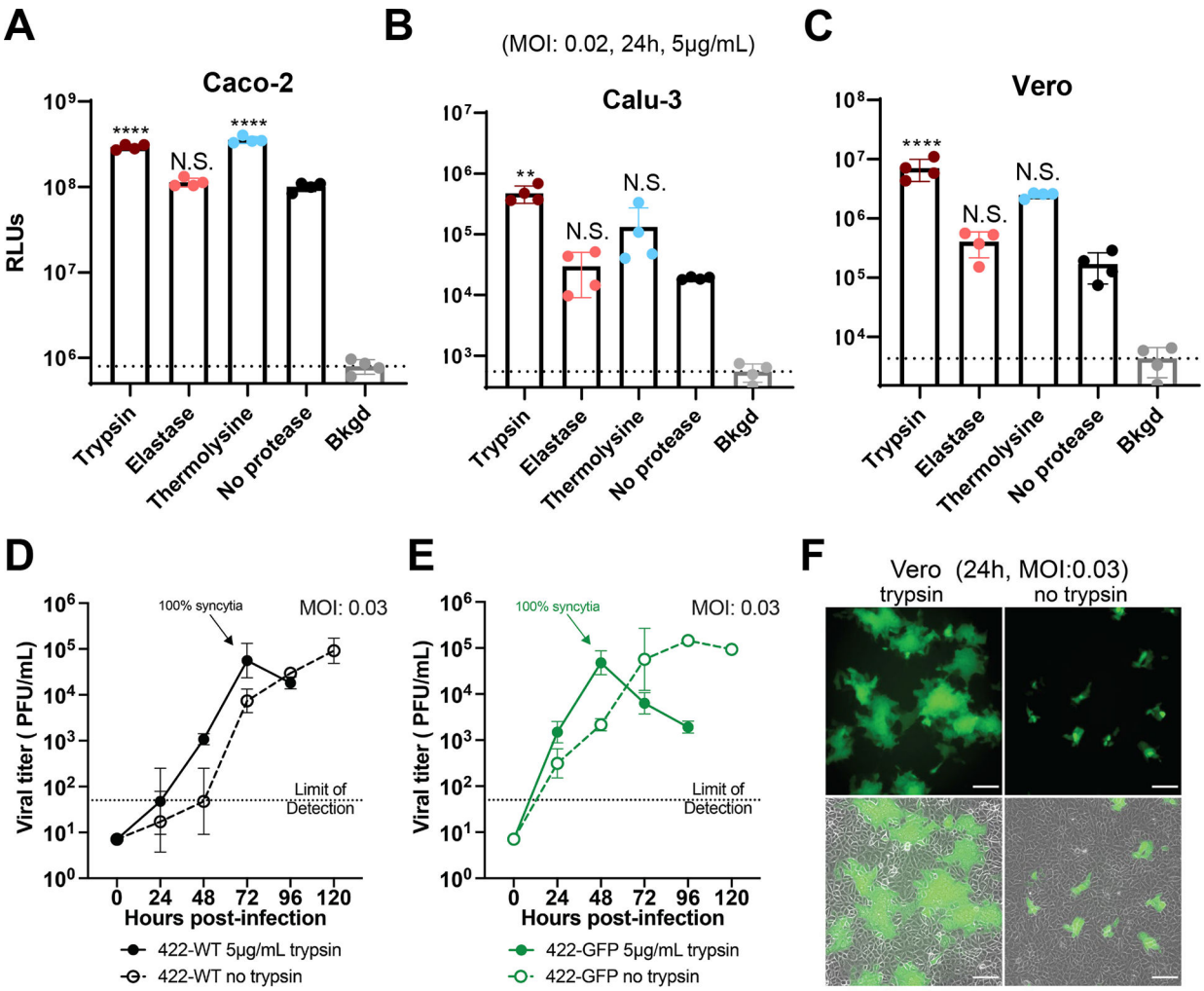

Figure 4. External proteases enhance BtCoV-422 replication and syncytia formation.

(**A to C**) Infection of BtCoV-422-nLuc (MOI: 0.02) was measured in Caco-2 (A), Calu3 (B), and Vero (C) cells in the presence of trypsin, elastase, or thermolysin. Nano luciferase activity were measured at 24hpi and reported as RLUs. Bkgd indicates background luminescence and is represented by the dotted horizontal line. RLUs were compared using one-way ANOVA to no protease control. N.S., not significant; **P< 0.01; ****P < 0.0001. (**D and E**) Growth kinetics were measured for BtCoV-422-WT (D) and BtCoV-422-GFP (E) in Vero cells with or without addition of trypsin. (**F**) Representative images are shown for BtCoV-422-GFP-infected Vero cells at 24 hours with or without addition of trypsin (Top row: no bright field; Bottom row: with bright field). Syncytia formation is observed in the trypsin-containing cultures. Scale bars indicate 200 μm. The data are presented as mean ± SD.

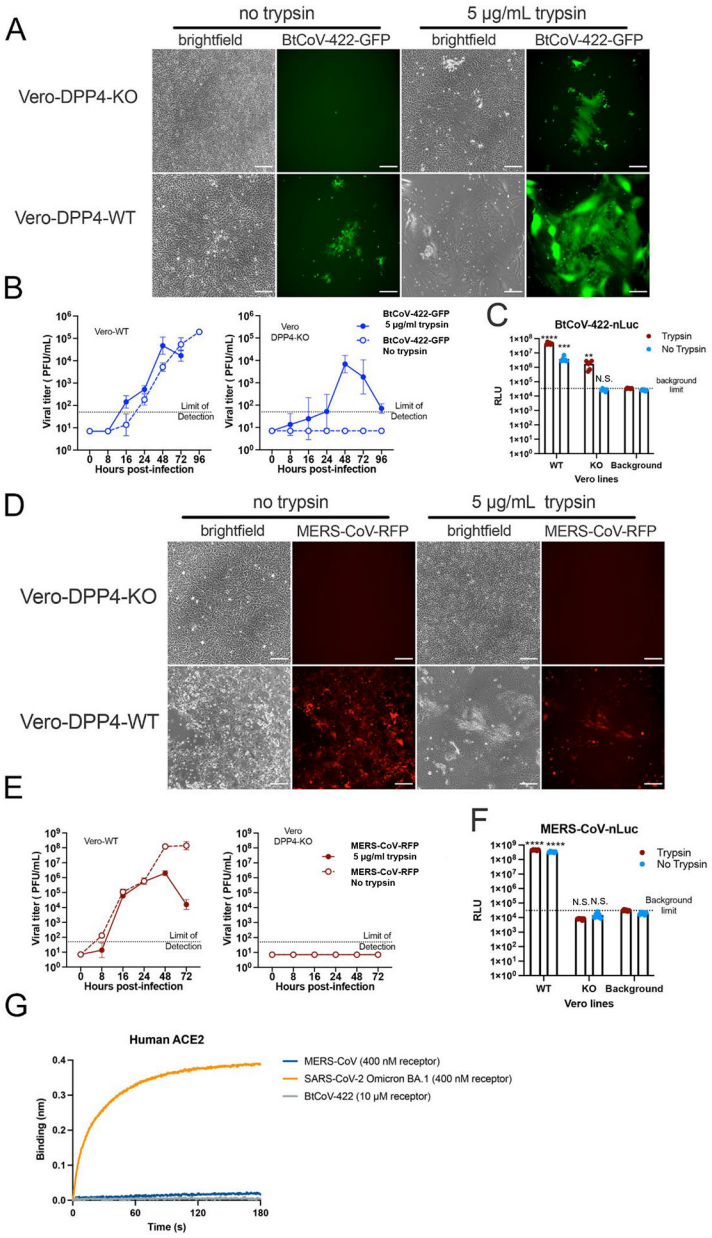

Figure 5. BtCoV-422 uses alternative, DPP4-independent pathways to enter cells in the presence of trypsin.

(**A and B**) Representative brightfield and BtCoV-422-GFP fluorescence images (A) and growth curves (B) are shown for BtCoV-422-GFP infection of in Vero DPP4 KO or WT cells, with or without trypsin. (**C**) Infection of Vero DPP4 KO or WT cells by BtCoV-422-nLuc, with or without trypsin, was measured by luciferase activity at 24 hours post infection. (**D and E**) Representative brightfield and MERS-CoV-RFP fluorescent images (D) and growth curves (E) are shown for MERS-CoV-RFP infection of Vero DPP4 KO or WT cells, with or without trypsin. (**F**) Infection of Vero DPP4 KO or WT cells by MERS-CoV-nLuc with or without trypsin, was measured by luciferase activity at 24 h post infection. Fluorescent images were taken at 48hpi with an MOI of 0.05. Scale bars indicate 200 μm RLUs were compared using non-parametric t-test compared with the corresponding

background values background signal in the corresponding condition. N.S., not significant; **P< 0.01; ***P < 0.001; ****P < 0.0001. The data are presented as mean ± SD. (**G**) Shown are biolayer interferometry measurements of MERS-CoV, SARS-CoV-2 Omicron BA.1, and BtCoV-422 spike proteins on a streptavidin biosensor dipped into human ACE2 for 180 seconds.

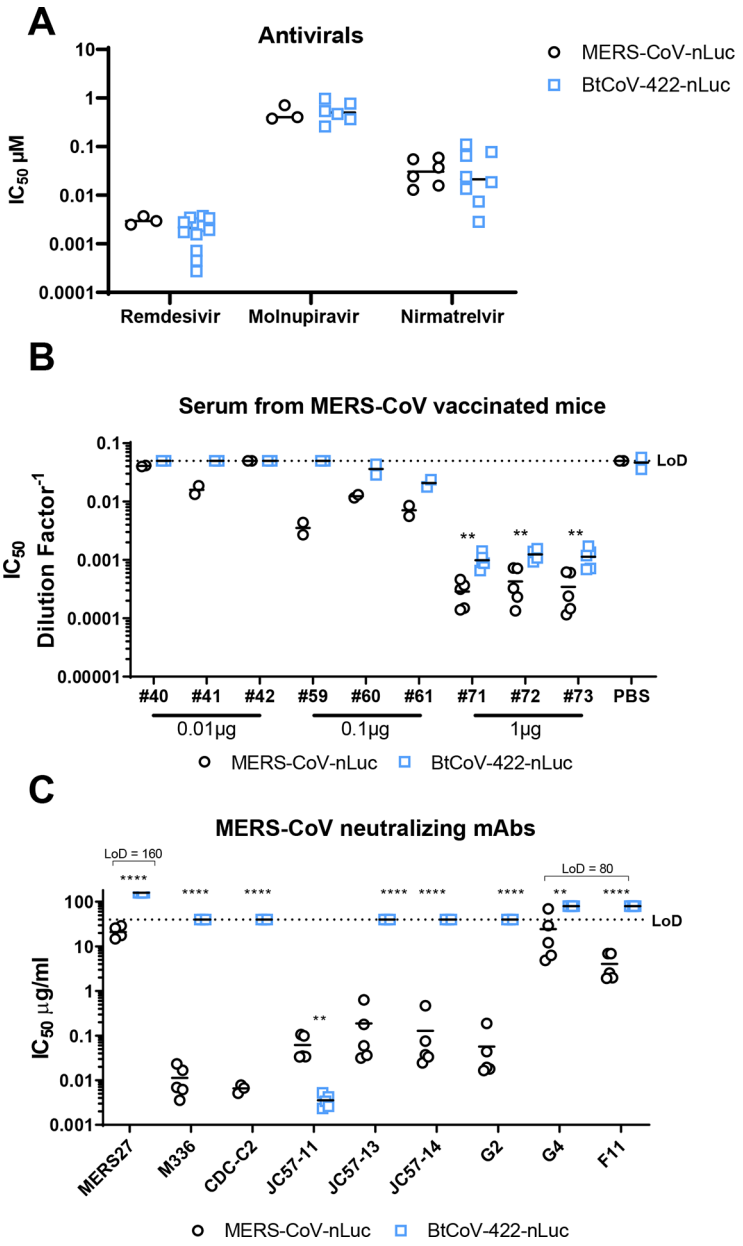

Figure 6. In vitro potencies of MERS-CoV-vaccinated mouse serum, neutralizing mAbs, and antivirals against BtCoV-422 in Huh7.5 cells.

(**A**) Inhibition concentration 50 (IC_{50}) values are shown for BtCoV-422 and MERS-CoV replication in the presence of remdesivir, molnupiravir, and nirmatrelvir in Huh7.5 cells. Quantitation of BtCoV-422 replication was measured by nLuc activity in technical triplicates. IC_{50} values are shown above. (**B and C**) Nano-luciferase based neutralization assays of MERS-CoV-nLuc and BtCoV-422-nLuc was performed using serum from mice immunized with a MERS-CoV-S2P mRNA vaccine (B) and a panel of neutralizing mAbs against MERS-CoV spike protein (C). Data are presented in (B and C) as IC_{50} values. The numbers in (B) indicate individual mice vaccinated with different doses. Serum from mock PBS-vaccinated mice were used as a control in (B). LoD indicates limit of detection at 40 µg/ml, unless specified in the graph. IC_{50} between BtCoV-422 and MERS-CoV were

compared using Student's t-test. **P< 0.01; ****P < 0.0001. Horizontal bars indicate mean values.

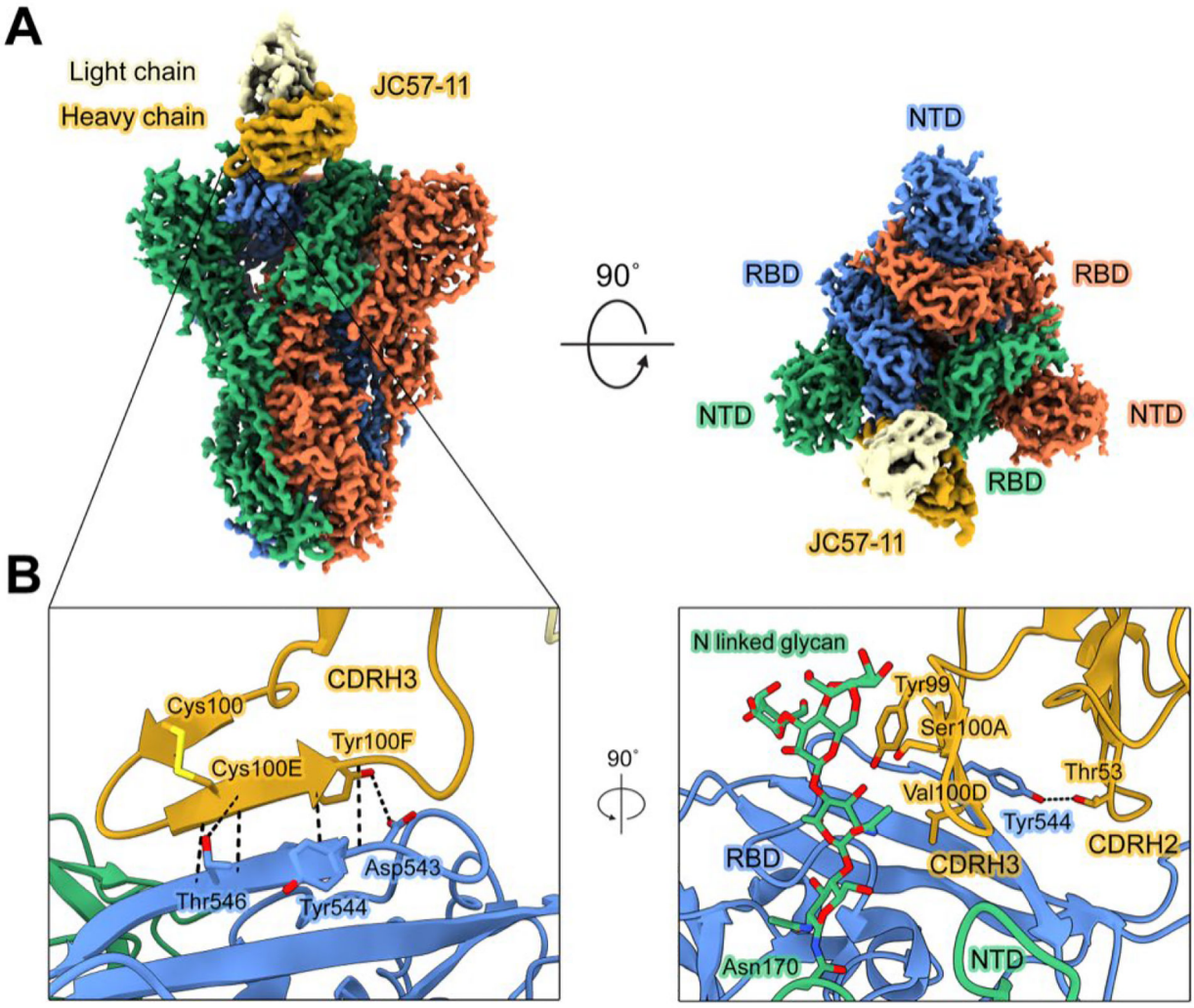

Figure 7. Cryo-EM structure of BtCoV-422 RBD and JC57–11 complex.

(**A**) Shown is the composite cryo-EM map of JC57–11 (EMD-40272, PDB 8SAK) bound to the RBD of the BtCoV-422 spike protein viewed from the side (left) and down toward the membrane (right). Spike protein protomers are colored orange, blue, and green. The heavy chain of JC75–11 is colored yellow, and the light chain is colored tan. (**B**) Shown is a model of the binding interfaces between JC57–11 and BtCoV-422 RBD. Interacting side chains are depicted as sticks. Hydrogen bonds are depicted as black dotted lines. Oxygen atoms are colored red, nitrogen atoms are colored blue, and sulfur atoms are colored yellow.